Ö. AKDENİZ

DESIGN AND IMPLEMENTATION OF A PLANETARY GEARBOX FOR A MICRO HYBRID POWERTRAIN

THE GRADUATE SCHOOL OF NATURAL AND APPLIED SCIENCES
OF
ATILIM UNIVERSITY

ÖZGÜR AKDENİZ

A MASTER OF SCIENCE THESIS
IN
THE DEPARTMENT OF MECHANICAL ENGINEERING

SEPTEMBER 2025

ATILIM ÜNİVERSİTESİ 2025

DESIGN AND IMPLEMENTATION OF A PLANETARY GEARBOX FOR A MICRO HYBRID POWERTRAIN

A THESIS SUBMITTED TO
THE GRADUATE SCHOOL OF NATURAL AND APPLIED SCIENCES
OF
ATILIM UNIVERSITY

BY

ÖZGÜR AKDENİZ

IN PARTIAL FULFILLMENT OF THE REQUIREMENTS
FOR
THE DEGREE OF MASTER OF SCIENCE
IN
THE DEPARTMENT OF MECHANICAL ENGINEERING

SEPTEMBER 2025

Approval of the Graduate School of Natural and Applied Sciences, Atılım University.

Assoc. Prof. Dr. Gökhan TUNÇ
Director

I certify that this thesis satisfies all the requirements as a thesis for the degree of **Master of Science in Mechanical Engineering, Atılım University**.

Prof. Dr. Hasan U. AKAY
Acting Head of Department

This is to certify that we have read the thesis DESIGN AND IMPLEMENTATION OF A PLANETARY GEARBOX FOR A MICRO HYBRID POWERTRAIN submitted by ÖZGÜR AKDENİZ and that in our opinion it is fully adequate, in scope and quality, as a thesis for the degree of Master of Science.

Asst. Prof. Dr. Ali EMİN
Supervisor

Examining Committee Members:

Prof. Dr. Hasan U. AKAY
Department of Automotive Eng.
Atılım University

Asst. Prof. Dr. Ali EMİN
Department of Automotive Eng.
Atılım University

Asst. Prof. Dr. Ramin BARZEGAR
Department of Mechanical Eng.
Hacettepe University

Date: *26 September,2025*

I hereby declare that all information in this document has been obtained and presented in accordance with academic rules and ethical conduct. I also declare that, as required by these rules and conduct, I have fully cited and referenced all material and results that are not original to this work.

Name, Last Name: Özgür AKDENİZ

Signature:

ABSTRACT

DESIGN AND IMPLEMENTATION OF A PLANETARY GEARBOX FOR A MICRO HYBRID POWERTRAIN

Özgür, AKDENİZ

M.S.., Department of Mechanical Engineering

Supervisor: Asst. Prof. Dr. Ali EMİN

September 2025, 76 pages

This setup aims to design, manufacture, and test a planetary gearbox to integrate a 3 HP electrical motor (EM) with an existing 20 HP internal combustion engine (ICE), creating a hybrid powertrain to reduce fuel consumption. A planetary gearset system can be used as a mechanical coupler between two separate power units, allowing their input speeds to be combined at the output. A second advantage of the planetary gearset lies in its high efficiency and significant gear-reduction potential, enabling two separate power units with different operating bands to operate seamlessly. Using the Goodman Criterion, a mathematical model was constructed in MATLAB, and the parameters obtained from the results were applied to design, model, and manufacture the devised planetary gearbox coupler. The gearbox was analyzed using dedicated engineering software, which verified a safety factor of 2.5 or higher and a projected service life exceeding 12,000 hours. A testing procedure was developed to determine the gearbox's efficiency after integration into the hybrid powertrain, and measurements were taken for two different connection ports. Using an EM, the tests were conducted with power figures up to 1 kW. The efficiency of the gearbox was measured experimentally to be around 60% for ring-carrier powerline and around 80% for sun-carrier powerline. Finally, a parallel hybrid electric vehicle (PHEV) simulation was conducted using the validated powertrain model and measured gearbox efficiency to evaluate the potential reduction in fuel consumption achieved by the proposed PHEV configuration. The simulation results show that PHEV design reduces the fuel consumption by 22% if the

ICE is connected to ring gear and 39% if the ICE is connected to the sun gear when compared with an equivalent conventional vehicle, with the planetary gearbox used for the mechanical coupler between the power units on the PHEV setups.

Keywords: Planetary Gearset, Powertrain, Hybrid, Parallel Hybrid, Hybridization, Fuel Consumption

ÖZ

MIKRO HIBRIT GÜÇ AKTARMA SISTEMI IÇIN PLANET DIŞLI KUTUSUNUN TASARIMI VE UYGULAMASI

Özgür, AKDENİZ

Y.L., Makine Mühendisliği Bölümü

Tez Yöneticisi: Dr. Öğr. Üyesi Ali EMİN

Eylül 2025, 76 sayfa

Bu çalışma, yakıt tüketimini azaltmak amacıyla 3 HP elektrik motorunu (EM) mevcut 20 HP içten yanmalı motor (ICE) ile entegre ederek hibrit bir güç aktarma sistemi oluşturmak için bir planet dişli kutusunun tasarımını, imalatını ve testini hedeflemektedir. Planet dişli sistemi, iki ayrı güç ünitesinin giriş devirlerini çıkışta birleştirebilen mekanik bir kaplin olarak kullanılabilir. Planet dişli kutusunun bir diğer avantajı ise yüksek verimliliği ve önemli dişli küçültme potansiyelidir; bu sayede farklı çalışma aralıklarına sahip iki ayrı güç ünitesi kesintisiz biçimde çalışabilir. Goodman Kriteri kullanılarak MATLAB ortamında matematiksel bir model oluşturulmuş ve elde edilen parametreler, tasarım, modelleme ve imalat aşamalarında uygulanmıştır. Dişli kutusu, özel mühendislik yazılımları kullanılarak analiz edilmiş ve 2.5 veya daha yüksek bir emniyet katsayısı ile 12,000 saati aşan bir hizmet ömrüne sahip olduğu doğrulanmıştır. Hibrit güç aktarma sistemine entegrasyonun ardından dişli kutusunun verimliliğini belirlemek amacıyla bir test prosedürü geliştirilmiş ve iki farklı bağlantı noktası için ölçümler yapılmıştır. EM kullanılarak yapılan testlerde 1 kW'a kadar güç değerleri uygulanmıştır. Dişli kutusunun verimliliği deneysel olarak halka taşıyıcılı enerji hattı için %60 civarında ve güneş taşıyıcılı enerji hattı için %80 civarında olacak şekilde ölçülmüştür. Son olarak, önerilen PHEV konfigürasyonu ile yakıt tüketiminde elde edilen potansiyel azalmayı değerlendirmek için doğrulanmış güç aktarma sistemi modeli ve ölçülen dişli kutusu verimliliği kullanılarak bir paralel hibrit elektrikli araç (PHEV) simülasyonu gerçekleştirildi. Simülasyon sonuçları, PHEV

tasarımının, PHEV kurulumlarındaki güç üniteleri arasındaki mekanik bağlantı için kullanılan planet dişli kutusuyla eşdeğer geleneksel bir araçla karşılaştırıldığında, içten yanmalı motor ayna dişlisine bağlıysa yakıt tüketimini %22 ve içten yanmalı motor güneş dişlisine bağlıysa %39 oranında azalttığını göstermektedir.

Anahtar kelimeler: Planet Dişli Seti, Güç Aktarma Organları, Hibrit, Paralel Hibrit, Yakıt Tüketimi

To my family,
who have been my most profound inspirations.

ACKNOWLEDGEMENTS

I would like to express my sincere gratitude to my supervisor Asst. Prof. Dr. Ali EMİN for his valuable guidance and support along with his encouragement, advice and insight throughout the course of this thesis, along with other studies.

I shall also thank to the members of my jury members, Prof. Dr. Hasan U. AKAY, Asst. Prof. Dr. Ramin BARZEGAR for their valuable criticisms and their valuable insights.

Furthermore, I thank the Automotive Engineering lab technician Ferdi GEZER for his valuable practical knowledge during the assembly and testing procedures.

Finally, I would like to present my thorough gratitude towards my parents, sister, my dear family along with my close firends for their endless support and encouragement during each step of this study.

TABLE OF CONTENTS

LIST OF TABLES

TABLES

LIST OF FIGURES

FIGURES

LIST OF SYMBOLS/ABBREVIATIONS

Roman Letter Symbols

i_g	Gear ratio factor	
k_x	Gear ratio for gear number x	
mG	Gear Module	
N	Number of teeth on gear	
n_b	Bending Safety Factor	
n_c	Contact Safety Factor	
R	Radius	m
T	Torque	N·m
Z	Number of teeth on gear	

Greek Letter Symbols

σ_b	Bending Stress	$\mathrm{Psi/MPa}$
σ_c	Contact Stress	$\mathrm{Psi/MPa}$
w	Rotational Velocity	$\mathrm{rad\,s^{-1}}$
η	Efficiency	
ϕ	Gear Pressure Angle	$^\circ$

Acronyms

CO_2	Carbon Dioxide
H_2	Hydrogen
BEV	Battery Electric Vehicle
CAD	Computer Aided Design
CE	Combustion Engine
EM	Electric Motor
FCEV	Fuel Cell Electric Vehicle
FHEV	Full Hybrid Electric Vehicle
ICE	Internal Combustion Engine
ICEV	Internal Combustion Engine Vehicle
PHEV	Parallel Hybrid Electric Vehicle

CHAPTER 1

INTRODUCTION

1.1. General

Land vehicles have been using internal combustion engines (ICE) since 1886 with the introduction of Benz Patent Motorwagen. The reason for their widespread use since then are for a couple of reasons. Their technology has matured and widely adapted over this course, making their production easy and cheap, lowering their initial purchase price. Then, their mechanical nature mean their maintenance, although not as easy as before, is still relatively easy, making their adaptation in rural or remote regions, along with third world countries, easier, resulting in their widespread use. Also, their choice of fuels mean they can store and carry a lot of energy which can be turned to propulsion since gasoline, one of the most popular fuel for passenger vehicles, contain around 10MJ of energy per liter [1]. However, fuel prices have increased dramatically over the last 30 years, which offsets the lower initial purchase price and the polluting nature of ICEs means that their ecological sustainability is questionable. Also, another issue present with ICEs is that they are working efficiently on a narrow rpm band, which is hard to achieve on real-life driving scenarios and often forced to work outside these rpm bands, resulting in increased fuel consumption. This is especially present in urban driving scenarios, where older petrol engines can have a fuel consumption figure twice the amount compared to long distance highway driving.

A possible solution for these issues is devised in the form of battery electric vehicles (BEV) since they theoretically provide a solution for these issues with reduced running costs by using electric motors (EM), which are more efficient than ICEs, that offer a flexible torque and power band. Thanks to this, if geared correctly, EMs can work inside its efficient region for most of the driving scenarios, especially in urban environments, offering a huge efficiency advantage when compared to ICEVs. A study shows that, BEVs are found to have a tank (or battery) to wheel efficiency between 50-80%, whereas the equivalent ICEV would have a tank to wheel efficiency of 14-33% for petrol and 28-42% for diesel variants [2]. Another study also points out that when looked at energy consumption values for an averagely sized ICEV and BEV, their

energy consumption values differ significantly. For example, a 1.6L petrol powered Hyundai Accent requires 57-62 kWh per 100km where the Nissan Leaf only requires 15-20kWh per 100km on the same test route [3]. The usage of electric motors also means zero tailpipe emissions and, therefore, zero local emissions.

However, they have several problems that have the potential to hamper their viability as a solution. First, most BEVs require at least considerable modifications to the vehicle platform for safety reasons, as the battery pack is required to be protected from impacts and deformations because of the fire and explosion risk it presents. In fact, in order to safely integrate the battery pack to the vehicle, the entire underbody is required to be modified to have a sandwich structure to house the battery pack as it was analyzed to be the safest option for the location of the battery pack as it was located inside the safety cell for the occupants of the vehicle, having the lowest risk for deformation, and subsequent physical damage which could lead to thermal runaway [4]. Second, the battery packs used on BEVs are required to be large. Most modern electric vehicles today, especially the more powerful variations, use lithium-iron-phosphate battery packs, which consist of hundreds of battery cells, creating packaging, safety and cost restrictions.

Despite the fact that lithium-iron-phosphate batteries currently have a class-leading energy density compared to other battery types, they still lag behind common fuels found in ICE, such as petrol or diesel, in terms of energy density by a margin of more than 20 to 1 [5]. This results in the phenomenon that to get meaningful range on a BEV, the battery pack capacity requirement is large enough to have a mass penalty of about 500kg when compared with their ICEV equivalents [6]. Then, each battery cell must be kept in the same state of charge and their charge-discharge rates controlled to make sure fire hazards, such as thermal runaway, or other hazards, do not occur [7]. For these reasons, the battery pack for the BEVs along with the custom platform required for the BEV results in them being considerably more expensive compared to their ICEV counterparts, costing upwards of 10,000 $ more [8]. Third, mostly because of the battery pack requirements, emissions created during production or BEVs are roughly twice the amount of ICEV equivalents, [9].

A big problem associated with this situation is that battery packs have a considerably lower lifespan compared to other components of the vehicle, amplifying this issue since battery packs account between 36-41% of the emissions of the vehicle during production phase [10]. Next, because BEVs use battery power only for their energy source, a dedicated charging infrastructure is required for them to be applicable for almost all applications, including urban applications where the user doesn't have access

to a household charging station. This hampers their feasibility and adaptability, especially for rural or remote regions where a dedicated charging infrastructure is difficult to implement.

A second option is to use Fuel Cell Electric Vehicles (FCEV) since they use EM for propulsion, just like BEVs. One critical advantage that they present is instead of using a big battery pack, they employ a hydrogen tank with a small battery pack, eliminating the need for a large battery pack and some of its shortcomings, such as thermal runaway or other similar hazards [7], along with manufacturing emissions related to battery packs, which is more than half of all production emissions related to BEVs [11]. Using Hydrogen (H_2) for fuel also mean that they do not need to be charged up with electricity, which could take anywhere between 30 minutes to 2 hours for an average BEV, using a 400kW DC rapid charging station. Instead, they can be filled up with H_2 in the same time it takes to fill up a conventional ICE car with the fuel of choice for the ICE. This allows them to have a shorter range than their BEV equivalents, since they don't have a charging anxiety issue present with BEVs, if sufficient fueling infrastructure is present. Also, they have a tank to wheel efficiency of about 46%, which is lower than BEVs, but higher than comparable ICEVs, with the numbers stated in the previous paragraph [12]. This allows for easier longer distance driving or more crucially, transporting heavy loads using lorries or semi-trucks with trailers.

However, they have unique challenges that need addressing for their viability. First, the structural integrity for the hydrogen tanks are just as important as they house H_2 in pressures up to 700 bars, creating a potential safety hazard in case of accidents as hydrogen is a flammable gas which can easily ignite [13]. This results in the need for a specialized or heavily modified platform, just like BEVs. A prime example of this is the Toyota Mirai, which is the most popular FCEV vehicle, that develops a unique platform to accomodate the hydrogen tanks safely in case of an accident [14]. Also, because these tanks hold heavily pressurized H_2, their lifespan is shorter than the average lifespan of the vehicle, not to mention costly. Second, although they are much easier and faster to fill up, they still need a dedicated fueling infrastructure which could safely store hydrogen. Although their numbers have increased, for example, in 2019, there were 52 stations in China up from just 2 a few years earlier, with a target of 1000 in 2030, and more are planned to open in the next few years, the number is far less than the current petrol, diesel and LPG fueling infrastructure [15]. Another big issue is the initial cost of the vehicle, which is considerably higher than comparable BEVs, with a €24,500 average premium required for FCEVs [13].

Another possible solution is devised to use Hybrid Electric Vehicles (HEV). They com-

bine an ICE with an EM, often smaller and less powerful than the ones found in BEVs and FCEVs. By combining and ICE with an EM, it is possible to obtain a powertrain which can be more efficient. There are distinctive advantages presented by HEVs. First, by combining an ICE with an EM, the ICE and the gearbox can be designed or tuned to work on high efficiency regions, reducing fuel consumption and greenhouse gas emissions (GHG). Second, unlike BEVs or FCEVs, a dedicated infrastructure isn't required at all for Micro Hybrid Electric Vehicles (MHEV) and Full Hybrid Electric Vehicles (FHEV), making its adaptation to non-developed countries or areas considerably easier. For Plug-in Hybrid Electric Vehicles (PiHEV), it is recommended to plug in the vehicle to minimize fuel consumption or use the vehicle as a BEV for short distance journeys. Third, by utilizing a much smaller battery pack, the initial purchase price of hybrids, especially MHEVs and FHEVs, are cheaper than their BEV equivalents in the U.S market [16].

However, hybrids do have their shortcomings. By utilizing an ICE with an EM, the overall amount of components, and thus, the complexity of the powertrain, is increased, making servicing the powertrain more difficult. Then, packaging can be a real constrain since an ICE, along with its components and an EM with a battery pack and drivers, along with other components are required. This issue is magnified in Plug-in Hybrid Electric Vehicles (PiHEV) since they use a larger capacity battery pack with larger EMs to be able to drive the vehicle on electric power alone for short journeys.

1.2. Motivation

When looked at the different solutions, it can be implied that HEVs, especially FHEVs or MHEVs offer the best solution, especially in regions without a dedicated charging or specialist fueling infrastructure. However, every new vehicle has an upfront cost which can be inaccessible for many people, especially in developing or third-world countries. Also, every new vehicle production creates a significant amount of emissions, which is unavoidable. A viable solution for these issues seem to be hybridization of existing vehicles. In theory, over 15% fuel consumption savings can be achieved by hybridizing existing vehicles [17].

To test this theory, a 1/5 scale model has been constructed, using a MHEV architecture and parallel hybrid as the hybridization method. The reason to choose MHEV over FHEV is to use a smaller EM to reduce costs and packaging constraints. Also, utilizing parallel hybrid rather than series hybrid as hybridization method has a couple of advantages for our application. First, it allows for both power sources to apply positive

torque to the wheels while having no energy conversion losses associated with the energy conversion process. Second, it allows for a comparatively compact setup thanks to the fact that smaller electric motors can be used than the ones found in series hybrid powertrains, without extra generators. However, for parallel hybrid powertrains, a mechanical coupling device is required [18]. Its prerequisites include durability, compact sizing while offering 2 power inputs and 1 power output port [18].

1.3. Scope of the Thesis

In this study, a planetary gearset system is devised as a solution for the coupler between 2 separate power sources in parallel hybrid powertrain setup because it allows 2 separate power sources to be coupled together without requiring a clutchpack or syncromesh gears because of its design, along with working with 2 different speed inputs since the gear ratios between sun, planet and ring gears create a gear reduction. [19]. Another advantage of the planetary gearset is the torque and speed addition to the output shaft, required for parallel hybrid powertrains.[18]. Checking real-life examples prove this point as they generally employ planetary gearboxes as a mechanical coupler between 2 separate power sources, like between a petrol engine and an electric motor. For this reason, a planetary gearset system is devised to be used as the coupler.

In order to design a planetary gearbox to test this theory, a mathematical model was built first to accurately make the calculations for the gearbox components. Secondly, power, speed along with torque curves from each power unit was implemented to determine the gear ratios between different gearsets. Third, with this information, the forces and the resultant moments acting on each part of the gearbox is established. Then, the geometries for each one of the mechanical parts are determined according to the calculations. According to literature research, in automotive applications, for gearboxes, a bending stress safety factor (n_b) between 1.1-3.2 and contact stress safety factor (n_c) between 1.1-2.6 is taken [20]. In order to be on the safe side, for this application, n_b is taken as 3.2 and n_c is taken as 2.6 minimum. Next, according to the calculation results, a correctly scaled CAD model of the gearbox is created using a 3D modeling program and technical drawings drawn according to the scaled 3D CAD model. The parts for the gearbox are manufactured or bought according to the technical drawings created. The assembly procedure is complete and the testing of the gearbox is currently being conducted.

To ensure the validity of the concept, a baseline consumption reduction figure is needed for comparison with the devised PHEV model. For that, a scaled PHEV model was

composed for powertrain system simulation first. For the model setup, parallel hybrid is chosen as the method for the hybridization of the powertrain for the reasons specified above. Another important reason is the overall compact size of the setup since no additional generator is needed and traction motors can be smaller than the ones found in series hybrid setups.

First, a baseline conventional vehicle powerline model is created using the opensource QSS-Toolbox in MATLAB/Simulink software. Second, a parallel hybrid setup was constructed. Third, the 1/5 scaled passenger vehicle parameters were integrated into the Simulink model to create a baseline model. Then, a custom planetary gearbox model was integrated into the model for the mechanical coupling between different power sources. Next, both models were run using NEDC driving cycles to ensure validity and proof of concept.

A consumption reduction figure of over 30% was achieved, which is much higher than the 15-20% reduction in fuel consumption according to the research conducted [17]. However, this model excluded some real life factors, one of the most important one of which was the efficiency of the gearbox designed for the coupling of the power units. In order to ensure we could prove the validity of the concept, a method for testing the efficiency of the gearbox is needed to be created.

CHAPTER 2

LITERATURE REVIEW

2.1. Powertrain Review

One of the most, if not the most, dominant power-plants for just about any land vehicle since late 19th century consist of a form of ICEs, owing to its matured technology and high power and torque capabilities. However, its reliance on oil, which can only be found on certain regions. This can create logistical and political challenges, not to mention a potential for price volatility, which can be a serious detriment for end users of ICEVs as in an atmosphere where price volatility can decrease consumer demand [21]. Also, the same literature research indicates that for every 10% price increase, consumer demand decreases between 3-10% and demand goes towards fuel-efficient alternatives [21]. Another research show that between 2000 and 2014, gasoline (or petrol) prices in 6 different regions vary by region or time, showing the volatility of the nature of fuel pricing [22]. The change in fuel prices throughout the years are presented in Figure 2.1.

One of the highest energy-related CO_2 emissions sector is transportation, following power, industry and agriculture sectors [23]. According to a literature study, it accounted to about 25% of all CO_2 emissions related to energy between 1997-2023 [24]. Another study determined than between 2011-2020, transport sector was responsible to about 27% of all CO_2 emissions [25]. Also, when looked at the CO_2 emissions trend, a study by [23] denotes the increasing trend from 5.1 Gtonnes (Gt) of carbon dioxide equivalent (CO_2-eq) in 1990 to 8.9 GtCO_2-eq in 2019, also showcasing the importance of land vehicles (excluding rail) as they account for a whopping 69% of all GHG emissions related to transportation. The emissions trends are denoted in the Figure 2.2.

A solution for these issues is presented in the form of pure BEVs. At first glance BEVs offer a great solution as instead of an ICE, they use one or more EMs to propel the vehicle without creating any local emissions and instead of using a fuel, like gasoline, they utilize a battery pack which needs to be charged as the vehicle is used. Another important advantage of EMs is that they can operate in a wide range of RPMs

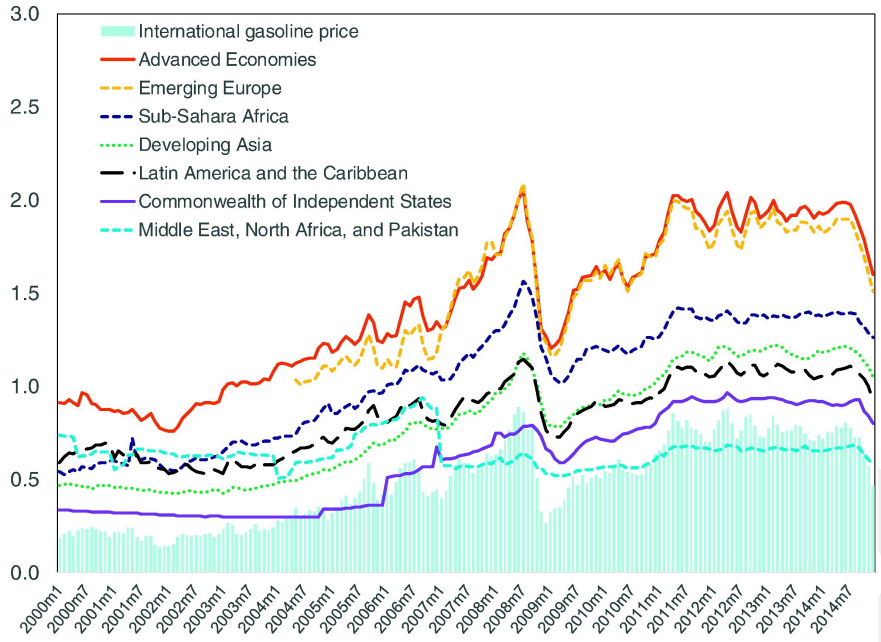

Figure 2.1 Change in Fuel Prices Throughout the Years [22]

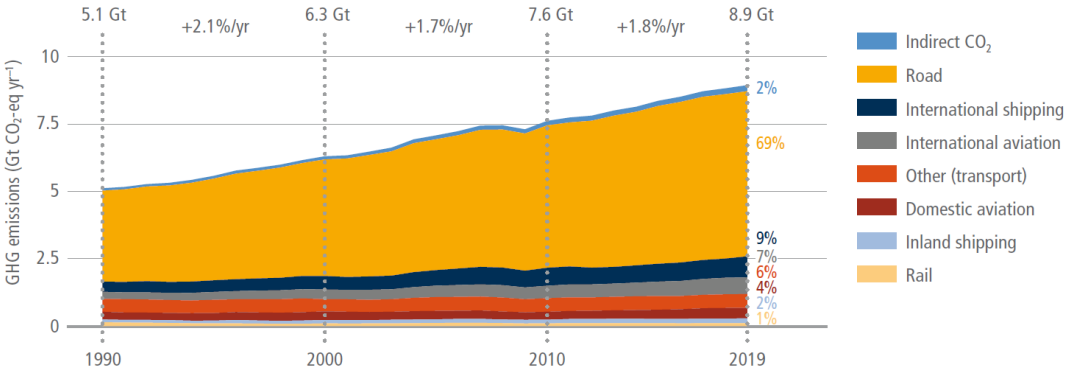

Figure 2.2 Global GHG Emissions Trends for Transport Sector [23]

efficiently, allowing them to operate without a dedicated gearbox for certain applications, simplifying the powertrain. Looking at literature studies it is possible to point out a considerable efficiency and energy consumption differences between ICEVs and BEVs. For instance, a study conducted by [2] showed that on average, BEVs had a battery to wheel efficiency ranging from 50-80%, which was much higher than equivalent ICEV models that had a tank to wheel efficiency range of 14-33% for petrol (or gasoline) models. Diesel models fared slightly better at 28-42%, still behind BEVs. Comparing real life examples show a similar trend. For example, on a predefined test route, a Nissan leaf has an energy consumption of 15-20 kWh whereas a similarly

sized Hyundai Accent with a 1.6 liter petrol engine and manual gearbox has an energy consumption of 57-62 kWh [3]. Also, they operate considerably quieter than ICEs, giving them a near-silent operation in which they can be used in urban areas without creating much disturbance.

However, they do have several shortcomings. First, their power and torque delivery is although wider than ICEs, without a gearbox they struggle with efficiency at highway speeds or if geared for highway driving, struggle with city driving, potentially necessitating at least a 2-stage gearbox for maximum efficiency. Also, their near-silent operation can actually create a safety hazard as it may become a challenge to detect an oncoming vehicle, resulting in an accident. Their main issue however, is the fact that, although they have zero local emissions, are actually not zero emissions vehicles at all. In fact, during their production, they create so much CO_2 that for a 150k km lifespan, it is estimated to have an impact equivalent to be 87 to 95 grams carbon dioxide equivalent per kilometer (g CO_2-eq/km), which is roughly twice the number for an equivalent ICEV production at just 43 g CO_2-eq/km [9]. Most of this difference comes from battery production, since mining the materials used in most batteries used on vehicles today require rare earth materials which are notoriously difficult and harmful to the environment during mining and processing. This is one of the main reasons why the battery packs, and therefore the vehicles, are considerably more expensive, upwards of 10,000 $ [8].

A second big disadvantage of the battery packs is energy density. Even though one of the most prominent battery chemistry technology in use today has a considerably better energy density than many other technologies employed just 15 years ago, they still have a massive gap behind several fuels currently in use by ICEs. When compared to petrol or diesel, their energy density is less than 5% of the aforementioned fuels. When looked at ethanol, this difference is less, but still high at around 6.25% [5]. The result is that to get a big enough battery pack, which is over 40 kWh to get meaningful range to make BEVs viable all-round options [26], the battery pack size needs to increase, creating packaging constraints big enough to necessitate platform modifications to accommodate the large sizes dictated by battery packs. Another issue related to this is the mass of the battery pack, which is high enough that, despite the absence of an ICE, gearbox and fuel tank, the overall mass penalty comes to around 500kg [6]. This is a big issue as 500 kg equates to a vehicle that is 2 classes bigger. For example, a 2017 Renault Zoe, a vehicle that has the same proportions as the Renault Clio and thus are located in the same segment (B hatchback), has around the same mass as the Renault Talisman, a vehicle that is 2 segments above (D saloon), and is

around 80 cm longer. This results in a situation in which the energy consumption of the vehicle, and therefore, the environmental impact, increases. Also, the consumption rate of the consumables, such as tires, increase as well, further increasing the environmental impact. Another issue related to lithium iron phosphate batteries is the risk of thermal runaways. To prevent such phenomena, or other safety related hazards, each individual cell needs to be kept at a certain temperature and state of charge to keep stability. Also, during charging and discharging, their charge and discharge rates need to be kept in check, along with their temperature to ensure the battery pack stays stable and hazardous situations, such as thermal runaways, don't occur [7]. For these reasons, it is also crucial to keep the battery pack safe and away from any deformations or crash forces to ensure thermal runaways or explosions don't occur. This requires significant platform modifications as protecting a large battery pack is an engineering challenge on its own.

A big problem associated with this situation is that, despite the fact that lithium iron phosphate battery packs have class leading charge and discharge rate and crucially amount capacities, they still have a considerably lower lifespan compared to other components of the vehicle, often losing 20% of capacity in just a few years, significantly reducing the range and usability of the vehicle. This is a big problem since they alone account between 36-41% of the emissions of the vehicle during production phase [10]. This amplifies the emissions issue as with a battery pack, even at 150000 km, a BEV still can't break even with a modern ICEV equivalent on an emissions scale.

Finally, because BEVs only use electric power from the battery packs to propel the vehicle, they require to be charged, and because battery energy density is considerably lower than common fuels, they require frequent charging, especially for long distance driving. This requires a considerable amount of time since an average battery pack requires over 30 minutes to be charged at a 400kW charging station, which is the highest charging option available today. This issue is small compared to the main problem, which is the fact that to use BEVs, a dedicated charging infrastructure is required on a scale which is at least comparable to the current fueling infrastructure. The only exception would be for urban only applications where the consumer has direct access to a household charging station, which is very rare as it requires private parking with access to electricity. This means that, in order to effectively adapt BEVs, a serious infrastructure investment is required, which is difficult to implement swiftly. This is especially problematic in developing or third world countries where implementing a wide scale charging infrastructure may not be feasible or economically viable. Also, rural and remote regions are another challenge for similar reasons.

To overcome these issues, HEVs can be utilised. With HEVs, the initial cost of vehicles can be significantly reduced to just a bit higher than their ICE counterparts [27]. Also, production emissions are significantly less than BEVs, and crucially, they do not have a requirement for dedicated charging infastructure [9]. This is made possible by using a much smaller battery pack, around 1-2 kWh for MHEVs and FHEVs and around 10-15 kWh for PiHEVs [28] instead of over 40kWh for BEVs [26] since hybrids combine ICE with and EM, eliminating the need for a large battery pack. This allows ICEs to operate in their efficient region while using the EMs for assistance. This makes hybrids, especially MHEVs and FHEVs less resource-intense than BEVs while being considerably more efficient than their ICEV counterparts [29].

An important advantage hybrids offer is that they offer considerable fuel consumption and emission benefits when compared to their ICEV equivalents by optimizing the use of available ICE. In fact, hybrids are shown to reduce fuel consumption and maintenance costs compared to their ICEV equivalents, along with reducing greenhouse gas emissions by 20-35% [9]. Another important factor is that, although BEVs can achieve lower emissions where the electrical grid is clean, HEV often outperform BEVs in coal-reliant grid regions [30], while considerably reducing local pollutants like NO_x and particulate matter compared to ICEVs [30]. Also, when looked at the total cost of ownership, HEVs consistently outperform their ICEV counterparts and rival their BEV counterparts, especially in cases where there are no subsidies or cheap charging solutions available [27].

Another advantage that the HEVs, esipecially MHEVs or FHEVs have over BEVs is that, since they don't require charging infrastructure and can simply use the available fueling infrastructure at hand, they can be rolled out easily and swiftly across different regions, including rural, remote regions along with developing zones, amplifying its advantages greatly [30]. Also, because they use conventional engines in an optimized manner, along with the readily available fueling infrastructure, it doesn't have a range or charging anxiety problem that BEVs currently have, or fueling anxiety that FCEVs have, which is another important problem for BEV or FCEV adoption [27]. For these reasons, HEVs, especially MHEVs or FHEVs currently fit existing infrastructure and consumer habits, making their adoption considerably easier and faster [29].

An important disadvantage of any brand new car is production emissions. On average, for a 150k lifespan an ICEV produces about 43 g CO2-eq/km [9]. This number is about 10-20 % higher for HEVs due to their extra components such as battery packs and electric motors [11], but the difference is relatively small when compared to BEVs over 100 %, often balancing out with less CO2 emissions values during vehicle operation

[31]. However, there are millions of pure ICEVs on the road today that, in theory, can be hybridized to avoid new vehicle production emissions, along with recycling emissions, not to mention the amount of energy required for these actions. This is made possible by the fact that hybrid vehicles often utilize same platforms and underpinnings as their pure ICEV counterparts. By hybridization, the production emissions can be kept as low as 0.5 tonnes of CO_2 since only hybrid-specific components are required [28]. This number is considerably lower than the 8.5 tonnes of CO_2e emitted and 102,000 MJ of energy required for the production of a Toyota Corolla model, which is an average sized, ICE only vehicle [32]. For these reasons, hybridization can offer a green solution. In the next section, hybrid types are discussed and the ideal hybrid architecture is determined.

2.2. Hybrid Types

As explained in the previous section, hybrid electric vehicles can provide an easy and quick solution to realistically reduce CO_2 emissions created by transportation sector. There are two main architecture types of hybrid powertrains in vehicle applications, which are series and parallel. Each have their distinctive advantages and disadvantages.

Series hybrid architecture relies only on EM for propulsion while the ICE works as a generator [18]. The most common configuration is given in Figure 2.3, where the electric motor is connected to the traction wheels and the ICE is coupled only to the generator. A rectifier is used to convert the mechanical power output of the ICE to electricity to charge the battery pack. This architecture originally came from an EV architecture where an ICE is added as a generator to extend the operational range of the vehicle because of the poor energy density of batteries [18]. Studies by [33] show that series hybrid powertrain applications are suitable for urban transit vehicles and buses, vehicles that are known to idle frequently and have variable-loads during driving, not ideal for ICE efficiency.

Some of the advantages of series hybrid powertrains include the following:

- No mechanical connection between the ICE and drive wheels, allowing the ICE to be used at its most-efficient region [18].
- Since EMs can have a near-ideal for traction torque-speed profile, a multi-gear transmisson isn't required for several applications, simplifying the drivetrain [34].

However, there are some distinct disadvantages of series hybrid configurations, which

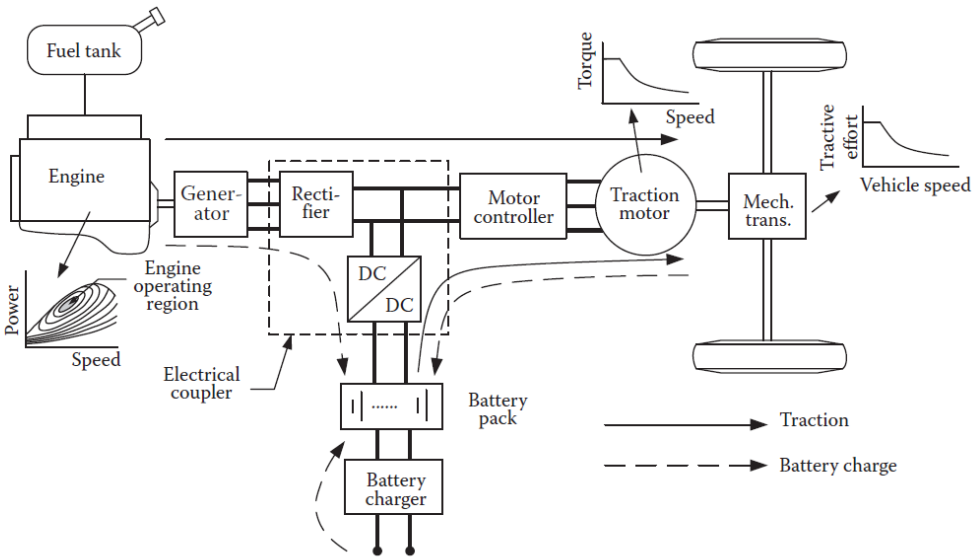

Figure 2.3 Configuration of a Series Hybrid Electric Drivetrain [18]

are the following:

- The engine's energy is converted twice (from mechanical to electrical and from electrical to mechanical), causing conversion losses, amplified in case of inefficient generator or traction motors [18].
- The generator adds additional cost and weight [18].
- The requirement for a bigger EM since it is the only motor that provides positive traction to the wheels [34].
- Using only the EM for propulsion means significant changes are required to adapt an existing ICE powered, conventional platform to use series-hybrid architecture, such as including different packaging and control systems [34].

Parallel hybrid on the other hand relies on both the ICE and EM for propulsion [18]. In the Figure 2.4, the most common configuration is presented, where the ICE is used to propel the vehicle, similar to the conventional ICE powered vehicles, with the EM working to assist the ICE, which is mechanically coupled to the driveline. The distinctive feature here is the mechanical coupling used to couple two separate power sources, where the ICE and EM have their speed and power outputs added on the output of the traction wheels [18]. Studies by [33] show that parallel-hybrid powertrains excel at highway and long-haul driving scenarios, where the ICE can perform more efficiently while the EM acts as an assistant during accelerations. Parallel-hybrid pow-

ertrains have been used in several applications, including passenger cars and light duty vehicles, thanks to their flexibility in adapting to existing platforms and powertrains [35].

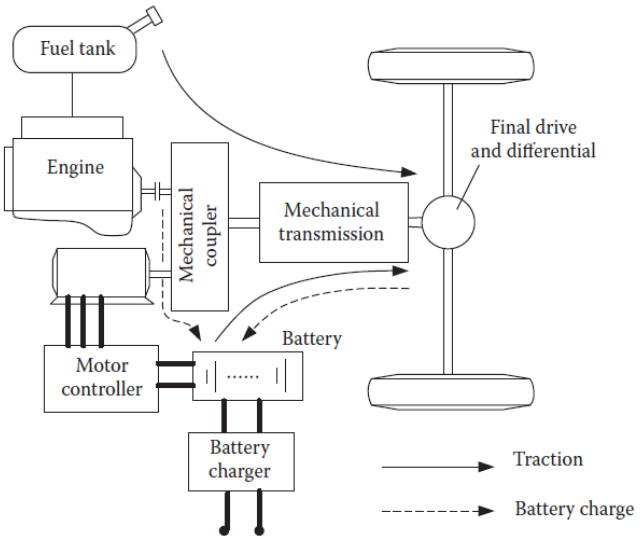

Figure 2.4 Configuration of a Parallel Hybrid Electric Drivetrain [18]

When compared to series-hybrid powertrains, parallel-hybrid powertrains offer the following advantages:

- Both power sources are connected to the traction wheels to provide positive traction, requiring a much smaller electric motor [35].
- Compact sizing since no additional generators are required [18].
- Easy to adapt to existing platforms and powertrains [35].
- Better accelerative performance and reduced fuel consumption in mixed driving cycles [36].

However, parallel-hybrid powertrains have a distinctive disadvantage:

- The requirement of a mechanical coupler between different power sources [18].

For the reasons above, parallel-hybrid for hybridization is a much easier and better solution than series-hybrid. However, the mechanical coupler is the main challenge that needs to be solved. In the next section some possible solutions are presented.

2.3. Planetary Gearbox

The main challenge in parallel-hybrid powertrains is the mechanical coupling between the EM and ICE. It needs to provide seamless coupling, power flow from 2 different inputs, and have speed summation properties. Planetary gearbox systems are one of the most common choice for this since they can combine two power inputs with torque or speed summation properties without requiring clutch packs or synchromesh. [37].

Planetary gearbox systems as couplers offer several advantages. They have a compact size and low mass relative to the torque distributed, thanks to its even load distribution across multiple planets. This results in lowered local stress points, lowering the risk of plastic deformation or fractures, ensuring reliability. A study was conducted using a combination of Lumped Parameter Method (LPM) and Finite Element Method (FEM) to accurately model and analyze the parts a multistage planetary gearbox system separately. The results were then compared with the calculations made to confirm the reliability of the analysis. The results showed that, the torque load was evenly shared across planet gears and in gears, the torque load was also distributed evenly across the gear surface, resulting in low local stress points, ensuring reliability and durabililty [38].

A second and a major advantage of planetary gearbox systems is that two separate power inputs can be used with different rotational velocities since two different reduction ratios can be applied to the inputs of the planetary gearbox and the power transitions can be conducted seamlessly without a syncromesh or clutchpack. A research study showed that, by connecting one of the power units to the sun gear and the other to the ring gear, it was possible to combine the speed and torque outputs of the power units, run each of them separately, or use one of the power units as a generator seamlessly [39].

Another study conducted by [40] showed the consistent behavior of a two stage planetary gearbox under different loads. An experimental setup was devised to test the planetary gearbox by running the gearbox for 30 seconds using constant speed and varying load. With this test, the dynamic torque, output speed and radial vibrations on the input and output shafts were observed. The results obtained from the experiments showed that, in different loads the planetary gearbox had a consistent performance, proving its usability. Also, the importance of lubrication was also shown as the gearbox was determined to have an efficiency of around 40% since it was run without any lubrication. A different study checked several planetary gearbox designs, and determined that load and torque sharing across planet gears was done evenly for the planetary gearbox

designs as long as no severe manufacturing errors were present. Another important factor determined was the fact that using 3 planets offered the best load and torque distribution, along with the lowest sensitivity to manufacturing defects, although tight tolerances and manufacturing standard requirements were still present [41].

A separate study conducted by [42] checked the robustness of the planetary gearbox system by checking constructing a dynamic model of the planetary gears using LPM. A modal analysis was conducted and vibration modes, along with natural frequencies of the planetary gears were checked. Then, another dynamic analysis was carried out using FEM to cross check and validate the results. In both analysis, parameters such as shaft flexibility, housing compliance, and tooth contact dynamics were considered. The results indicate that coupling performance is directly affected by resonance and vibration, making them crucial parameters in gearbox design. If these parameters are kept in check, the gearbox is proven otherwise to be robust for coupling two separate power units.

It was shown that, by optimizing the design, planetary gearbox systems can be made to have higher torsional stiffness, especially with correct bearing and carrier architectures. A gearbox design was optimized by FEM, using ANSYS analysis software, to imrprove strength, reduce fatigue and deformation, minimize mass and costs. Several designs were anayled and then optimized to achieve a 55% reduced deformation, 38% lower stress, along with 5% less mass than before, while eliminating weak bolt joints, minimizing local stress points and increasing load bearing efficiency [43].

However, planetary gearboxes have some distinct disadvantages that need to be considered. First of all, they are considerably more complex than many other coupling methods. When this is combined with the fact that sensitivity in manufacturing and assembly is crucial for correct and efficient operation of the gearbox, it can be difficult to achieve the desired efficiency values shown [39]. Another problem related to this situation is the fact that the cost of the manufacturing can be expensive, which can hamper applications where budget is a significant concern [41]. Another big issue is the fact that without proper optimization and resonance and vibrations kept unchecked, load sharing can get adversely affected, lowering the useful service life of the parts by creating local stress points [39]

There are some research on rectifying these shortcomings. It was shown that, by optimizing the design, planetary gearbox systems can be made to have higher torsional stiffness, especially with correct bearing and carrier architectures. A gearbox design was optimized by FEM, using ANSYS analysis software, to improve strength, reduce fatigue and deformation, minimize mass and costs. Several designs were analyzed and

then optimized to achieve a 55% reduced deformation, 38% lower stress, along with 5% less mass than before, while eliminating weak bolt joints, minimizing local stress points and increasing load bearing efficiency [43]. These phenomenons were proved by another research conducted by [44]. Both of the studies suggests the following methods:

- Improving load-sharing methods
- Using preloading methods
- Optimizing carrier geometries

With these methods applied, along with manufacturing processes carried out correctly, most of the shortcomings of a planetary gearset system can be rectified, resulting in a coupling method that has very few disadvantages and many advantages. For this reason, as shown by the studies conducted by [37] signify that several parallel and series-parallel hybrid powertrains use a planetary gearset as the coupling device between two power units.

2.4. Applications of Planetary Gearbox

When looked at the powertrain of real-life HEVs, planetary gearboxes are a dominant choice for mechanical coupling for different architectures and applications for the reasons explained above. Studies show that as long as manufacturing tolerances are followed, balancing done correctly and appropriate lubrication applied, the efficiency of the planetary gearbox can reach mechanical efficiency values over 90% [45]. Another research paper by [46] looked at HEV applications of planetary gearboxes, called as Planetary Hybrid Powertrain Systems (PHPS). This architecture allows power-splitting between an ICE and one or more EMs in an efficient manner. Several different powertrain configurations were checked, using one or two EMs, with 4 separate configurations for each, depending on the gearbox used by ICEs. It was determined that, as long as no manufacturing defects were present, efficiency for the gearbox was determined to be over 90%, which was higher than belt or fixed gear couplers and powertrain efficiency improvements of between 20-35% depending on control strategy were observed.

One of the earliest commercial applications for a planetary gearbox in a HEV powertrain is utilized in the THS-II hybrid power architecture found in third generation Toyota Prius. The planetary gearset is used as a power-split device in which it acts as the mechanical coupling between the ICE, generator and traction motor. In this appli-

cation, the gearbox was simulated and then tested. The mechanical efficiency of the gearbox was measured and calculated to be around 96% [45].

As a matter of fact, several real-life examples use a planetary gearbox for mechanical coupling between two power sources. They are listed in the Table 2.1.

Table 2.1 Planetary Gearbox Applications in Real Life Vehicles

HEV (Model & Year)	**Planetary Gearbox Application**	**Gearbox Efficiency**	**Efficiency Gain vs ICE**
Toyota Prius (2010, Gen-3)	Single-PG input-split e-CVT; ICE–MG1–MG2 coupled via PSD	96–97%	+72.4% vs 2010 Corolla (50 vs 29 mpg combined)
Toyota Camry Hybrid (2012)	Single-PG input-split e-CVT (Aisin PSD)	96–97%	+42.9% vs 2012 Camry 2.5L ICE (40 vs 28 mpg combined)
Ford Escape Hybrid (2009)	Single-PG input-split e-CVT (THS-derived PSD)	96–97%	+39.1% vs 2009 Escape ICE (32 vs 23 mpg combined)
Toyota Highlander Hybrid (2008)	Single-PG input-split e-CVT PSD	96–97%	+44% vs 2008 Highlander V6 4WD ICE (26 vs 18 mpg combined)
Generic HEV PSD hardware (bench tested)	2-DOF single PG tested as HEV power-split element	96–97%	Component-level test (not vehicle)
BMW ActiveHybrid 7 (2011)	ZF 8HP planetary automatic with integrated e-machine (parallel full hybrid)	98%	18% (20 vs 17 mpg combined)
Porsche Cayenne S Hybrid (2011)	Aisin 8-speed planetary automatic with integrated motor (parallel hybrid)	97–98%	17% (21 vs 18 mpg combined)
Audi Q5 Hybrid (2013)	8-speed planetary automatic (parallel hybrid)	97–98%	13% (27 vs 23 mpg combined)
Hyundai Sonata Hybrid (2012)	6-speed planetary automatic; motor replaces torque converter (parallel hybrid)	97–98%	29% (36 vs 28 mpg combined)
Kia Optima Hybrid (2014)	6-speed planetary automatic (parallel hybrid)	97–98%	32% (37–38 vs 28 mpg combined)
Mercedes-Benz E400 Hybrid (2013)	7G-Tronic PLUS planetary automatic with integrated motor (parallel hybrid)	97–98%	13% (26 vs 23 mpg combined)

CHAPTER 3

METHODOLOGY

A planetary gearset is determined to be the best solution for coupling two separate power units. The design of the gearbox was conducted with cost, modular design and ease of manufacturing as key points. MATLAB was used for creating a mathematical model, using Goodman Criterion to ensure calculations were verified. S-N curve and other criterions were considered, however the Goodman Criterion was determined to be used for our application as it has different equations and theorems to satisfy every stress and strain parameter found on each mechanical component inside the gearbox [47]. The calculations were made by hand to cross-check and validate the mathematical model created. With the results obtained from the calculations, a market research was conducted on several different materials to obtain its engineering data. With all of these values at hand, the specification of every single gearbox component was determined. A second software was also used to double-check the calculations to ensure its validity.

After the calculations are verified, using a CAD software, each component of the gearbox is modeled and then the assembly of the entire gearbox was done in 3D environment to ensure there were no conflicts. After the compatibility was verified, the design was frozen and technical drawings of each gearbox component was created. The parts were then manufactured according to the drawings. Then, the parts are assembled together according to the technical drawings. The gearbox was tested to ensure it was working as intended. Then, a leak-down test is being conducted to ensure there are no leaks coming from the gearbox to ensure sufficient amount of oil is present inside the gearbox to properly lubricate the gearbox at all times. Then, the gearbox is run without any dyno load to break-in the gears before being connected to the dyno for the gearbox testing.

To test the gearbox, we determined the inertia caused by the dynamometer first to ensure the tests would accurately show the efficiency of the gearbox. For that, a 2.2kW electric motor that will also be used in the hybrid powertrain was used. Several test points ranging from 100-2800 RPM were determined according to the literature survey conducted along with the RPM range of the tested electric motor [48]. Second,

with these test points in hand, the EM was tested first without being connected to the dyno, then the same tests were repeated with it being connected to the dyno to compare the results and create a baseline drag torque occured from the dynamometer [49]. After a baseline torque value for the dynamometer was determined, several tests were conducted on different load values to determine the efficiency map for the EM under different load tests as a baseline to compare for the gearbox [50]. After obtaining the efficiency map of the EM, the gearbox was connected to the dynamometer to do a series of load tests to determine its efficency across a different range of speeds and loads [51].

After determining the efficiency of the gearbox, a hybrid simulation setup in which the gearbox will be used as a speed coupler was created. For this, the opensource Qss-Toolbox in MATLAB Simulink is used. With this toolbox, a 1/5 scaled passenger vehicle parameters were calculated and integrated to the Simulink Model to create a base model in which the the hybrid powertrain will be applied. The reason to create a 1/5 scaled vehicle model is because of the chosen power units and their power and torque values corresponding to a 1/5 scaled passenger vehicle. Then, with the efficiency of the gearbox determined, the planetary gearbox was added as a coupler and gear reductor for the base and hybrid models. After adding the gearbox, with NEDC as the driving cycle as the testing procedure for real-life validity, both models were run, proving the concept and ensuring validity. Next, several parameters are checked to show the difference in ICE-only (conventional) or hybrid (PHEV) powertrains and a considerable fuel reduction of 36% was achieved.

3.1. Gearbox Design and Manufacturing

3.1.1. Principles of Planetary Gearset as Speed Coupler

The power output of two separate power units can be coupled together by speed summation method, meaning their speeds are added up. A mechanical coupler, like a planetary gearbox, can be used for this purpose as a speed coupler requires a three-port device with two inputs and one output [18]. One of the inputs have a unidirectional energy input and is denoted as port 1, where the ICE is connected. the other ports have bidirectional energy flow and can be connected to either the EM or the output [18]. For the sake of calculations, port 2 will be denoted as the EM input and port 3 will be denoted as the output. in the figure given below, you can see the schematic for a mechanical coupler working as a speed coupler.

The mechanical speed coupler shown here has the following property:

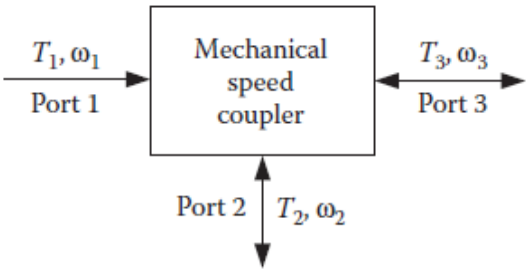

Figure 3.1 Schematic of a Mechanical Speed Coupler [18]

$$w_3 = k_1 w_1 + k_2 w_2 \tag{3.1}$$

where k_1 and k_2 values are constants, which are determined from the structural and geometrical design. Two of the three given speed values, w_1 w_2 and w_3, can be independently controlled. However, because of the constraint of power conservation, the torque values are linked together with the following correlation, where the minimum torque is used for determining the other torque values:

$$T_3 = \frac{T_1}{k_1} = \frac{T_2}{k_2} \tag{3.2}$$

One of the most common mechanical speed coupling device is the planetary gearset, a schematic of which is given in the figure below. A planetary gearset has three ports in which there is a sun gear, ring gear and yoke, labeled as 1,2 and 3 respectively. The following method can be utilized to obtain the speed relationship between the gears.

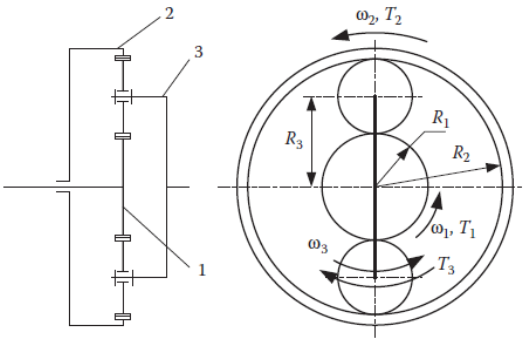

Figure 3.2 Schematic of a Planetary Gearset Used as a Speed Coupler [18]

To determine the gear ratios between the gears, a few scenarios will be defined. In the first scenario, the output side, also known as port 3 or yoke, will be made stationary,

that is $w_3 = 0$. From here, the gear ratio from the sun gear to the ring gear, denoted as $i^3_{1-2} = 0$, can be determined using the following relation:

$$i^3_{1-2} = \frac{w^3_2}{w^3_1} = -\frac{R_2}{R_1} = -\frac{Z_2}{Z_1} \tag{3.3}$$

Here, w^3_1 and w^3_2 are the angular velocity values of the sun gear and ring gear with respect to the yoke when $w_3 = 0$. The radius of the sun and ring gears are respectively denoted as R_1 and R_2, and the number of teeth of the sun and ring gears, that are also proportional to the radius of the sun and ring gears, respectively, are denoted as Z_1 and Z_2. In 3.2, the positive velocity is defined in the counterclockwise rotation direction. From equation 3.3, it can be determined that w^3_1 and w^3_2 have different rotational directions, giving the following i^3_{1-2} gear ratio as negative.

For the next step, when $w_3 \neq 0$, the gear ratio i^3_{1-2} can be denoted by the following equation:

$$i^3_{1-2} = \frac{w_1 - w_3}{w_2 - w_3} \tag{3.4}$$

Rearranging the equation gives the following:

$$w_1 - i^3_{1-2} w_2 - (1 - i^3_{1-2}) w_3 = 0 \tag{3.5}$$

As a general rule, a gear ratio can't be a negative value, for that reason the i^3_{1-2} gear ratio has to be defined as a positive value, given as

$$i_g = i^3_{1-2} = \frac{R_2}{R_1} = \frac{Z_2}{Z_1} \tag{3.6}$$

then the previous equation becomes

$$w_1 + i_g w_2 - (1 + i_g) w_3 = 0 \tag{3.7}$$

which can be rearranged as

$$w_3 = \frac{1}{1 + i_g} w_1 = \frac{i_g}{1 + i_g} w_2 \tag{3.8}$$

Combining 3.8 with 3.1 gives us $k_1 = \frac{1}{1+i_g}$ and $k_2 = \frac{i_g}{1+i_g}$.

Similarly, for the acting torque on the elements of the planetary gearset, when the counterclockwise rotation is defined as the positive orientation for applied torque and clockwise rotation is defined as the negative orientation, the total system power is assumed to be zero when frictional losses inside the unit are ignored, giving the following the relation

$$T_1 w_1 + T_2 w_2 + T_3 w_3 = 0 \tag{3.9}$$

Combining 3.8 with 3.9 gives the following

$$T_3 = -(1 + i_g) T_1 = -\frac{1 + i_g}{i_g} T_2 \tag{3.10}$$

From 3.10, T_1 and T_2 torques acting on sun and ring gear respectively, always are both positive or negative, with T_2, torque acting on the yoke or output, acting in the opposite direction to T_1 and T_2, also denoted in 3.2.

When one of the elements, either sun gear, ring gear or yoke, are fixed, reducing the degree of freedom, the gearset system becomes a gear reduction system with one input and one output. In the Table 3.1 below, the relationships between speed and torque are denoted with different parts fixed. These relations can be utilized to determine the efficiency of the planetary gearset coupling on different power flow lines.

Table 3.1 Speed and Torque Relationships While One Element is Fixed [18]

Element Fixed	**Speed**	**Torque**
Sun Gear	$w_3 = \frac{i_g}{1+i_g} w_2$	$T_3 = -\frac{1+i_g}{i_g} T_2$
Ring Gear	$w_3 = \frac{1}{1+i_g} w_1$	$T_3 = -(1 + i_g) T_1$
Yoke	$w_1 = -i_g w_2$	$T_1 = \frac{1}{i_g} T_2$

3.1.2. Mathematical Model

A mathematical model was created with Goodman Criterion for the calculations to determine our requirements for the coupling gearbox. MATLAB was used for constructing this model and it was cross checked with the example gearbox given in Chapter 18 of the Shigley's Engineering Design Book [47]. In Table 3.2 you can see the resultant dimensions for some of the mechanical components used for the gearbox.

Table 3.2 Gear Dimensions From the Example Study and Model [47]

Gear	Diameter from model (in)	Diameter from book (in)	Width from model (in)	Width from book (in)
2	2.67	2.67	1.5	1.5
3	12	12	1.5	1.5
4	2.67	2.67	2	2
5	12	12	2	2

The validity of the mathematical model was proven with these tests.

After the validity of the model was verified, modifications to it were made to ensure its compatibility with the requirements for this application. In the Table 3.3 the inputs are given.

Table 3.3 Input Values and Specifications for the Gearbox Application

Specification	Values
Gear Module (ig)	2.89
Input Speed (wi)	4000 RPM
Carrier Gear Teeth Number (N(3))	27
Sun Gear Teeth Number (N(2))	26
Internal Ring Gear Teeth Number (N(5))	78
Electric Motor (EM) Power rating (H1)	3 HP
Internal Combustion Engine (ICE) Power rating (H2)	20 HP
Gear pressure angle (phi)	20 °
mG	3
mN	1
SH	2
Sc	225 000 Psi for all gears
StB	65 000 Psi for all gears
Operation life (L(2-5))	12000 h

According to these inputs, the mathematical model was modified to suit our needs.

The dimensions of the gearbox will be 332mm*458mm*305mm,which is shown in Figure 3.3. It can be added after the gearbox in rear wheel drive vehicles.

3.1.3. Materials

Grade 2, carburized and hardened steel was used for the gears and its properties are taken from [47]. AISI 4140 steel was used for the shafts, whose properties are taken from [47]. Al 6061-T6 was used for the ring connector and arm that connects carrier gears with the hollow shaft and its properties are taken from [52]. Al 7075-T6 was

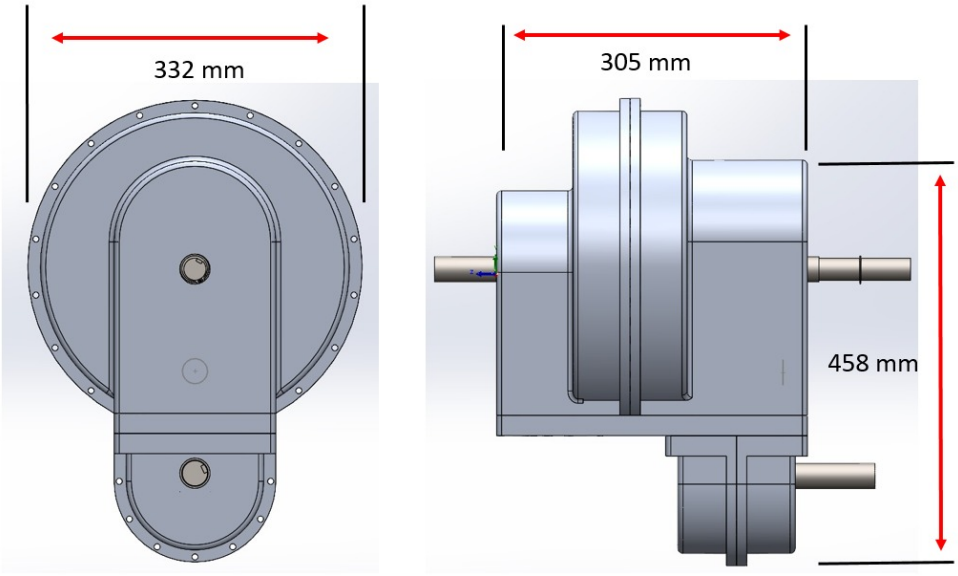

Figure 3.3 Dimensions of the Gearbox

used for the bearing housings and the floor of the gearbox and its properties are taken from [53]. Material properties for the gears and shafts are given in the Table 3.4 and for the aluminum parts are given in the Table 3.5.

Table 3.4 Properties of Materials Used on Construction of the Gears and Shafts

Specification	**Grade 2, carburized and hardened steel (Gears)**	**AISI 4140 steel (Shafts)**
Young's Modulus (MPa)	71000	200000
Poisson's Ratio	0.33	0.3
Allowable Bending Stress Number (ksi)	65	22
Allowable Contact Stress Number (ksi)	225	145

Table 3.5 Properties of Materials Used on Construction of Aluminum Parts

Specification	**Aluminium 6061-T6**	**Aluminum 7075-T6**
Young's Modulus (MPa)	71000	71000
Poisson's Ratio	0.33	0.33
Allowable Bending Stress Number (ksi)	26	75
Allowable Contact Stress Number (ksi)	35	81

3.1.4. Calculations

After validating our MATLAB model, Goodman Criterion was used for calculations for each mechanical part found on the gearbox with a minimum operating life of 12000 hours with the inputs given on the table from the previous section. All calculations were taken from the Shigley's Mechanical Engineering Reference Book [47]. Imperial units have been used in this section because of the similar design cases that are available in the reference book.

3.1.4.1. Torque, Loads, Speed

From the calculations found in [47], the transmitted torque, load and pitch line velocity values are calculated and provided in the table 3.6.

Table 3.6 Transmitted Torque, Load and Pitch Line Velocity From the Gears

Transmitted Parameter	**Carrier**	**Sun**	**Ring**
Torque (T)	15.10 lb.ft	3.94 lb.ft	26.3lb.ft
Transmitted Load (Wt)	250.89 lbf	31.51 lbf	72.72 lbf
Pitch Line Velocity (V)	3.02×10^3 ft/min	3.14×10^3 ft/min	9.07×10^3 ft/min

With all these parameters, gear and shaft calculations can be made according to these values.

3.1.4.2. Gears

The calculations from [47] are used for calculating the safety factors for the gears using Imperial units. The parameters other than the input parameters taken for the calculations are given in Table 3.7. These parameters are taken according to the gear type and design parameters, along with production methods and AGMA/ISO standards.

Using these constants, along with the formulas given in [47], the stress and therefore, the safety factors can be determined. They are given in Table 3.8:

From these calculations, the minimum safety factors were determined on the the carrier gears, equal to of 2.73 for n_c and 8.59 for n_b were found, which is more than the minimum desired safety factor of 2.6 for n_c and 3.2 for n_b [20]. For the other gears, higher safety factors were obtained, making this design safe for these application parameters.

Table 3.7 Load Parameter Constants of Gears

Specification	**Values**
Quality Number Q_v	7
Face Load Distribution Factor Constant C_{mc}	1
Face Load Distribution Factor Constant C_{pm}	1
Face Load Distribution Factor Constant C_e	1
Elastic Coefficient for Steel C_p	2300
Empirical Constant A	0.127
Empirical Constant B	0.158
Empirical Constant C	-0.930×10^{-4}

Table 3.8 Stress and Safety Factors of Gears

	Carrier	**Sun**	**Ring**
Contact Stress σ_c	59.88 ksi	35.15 ksi	22.43 ksi
Bending Stress σ_c	66.39 ksi	25.12 ksi	42.57 ksi
Contact Safety Factor n_c	2.73	4.53	7.30
Bending Safety Factor n_b	8.59	22.71	13.40

3.1.4.3. Shafts

After calculating the gears, the same calculations were carried out for the shafts to ensure they are up to the same standars as the gears. In this gearbox application, there are 6 distinctive shafts available with different geometries, loading values and fixtures. The layout of the shafts are denoted in the Figure 3.4

Shaft 4 is chosen for the shaft calculations since it is subjected to the highest amount of loads and torques of the present shafts. A free body diagram is drawn of the shaft first, which is given below.

After determining the forces and their application points, the stress concentration points are determined. Then, several constants are determined according to the design parameters, ISO/AGMA standards and [47]. Those parameters for the concentration points on the shaft #4 are given in table 3.9.

With the forces and its locations known, the torque and moments are calculated. Then, with these values, the critical points are determined and the stress values on those points are calculated. Then, these calculations are repeated for other shafts.,With those values, along with diameters of the shafts known, the safety factors of the shafts are determined. All of the calculated values are given in Table 3.10.

From the obtained results, shaft 1 and 2 have the minimum safety factor of 8.59, which

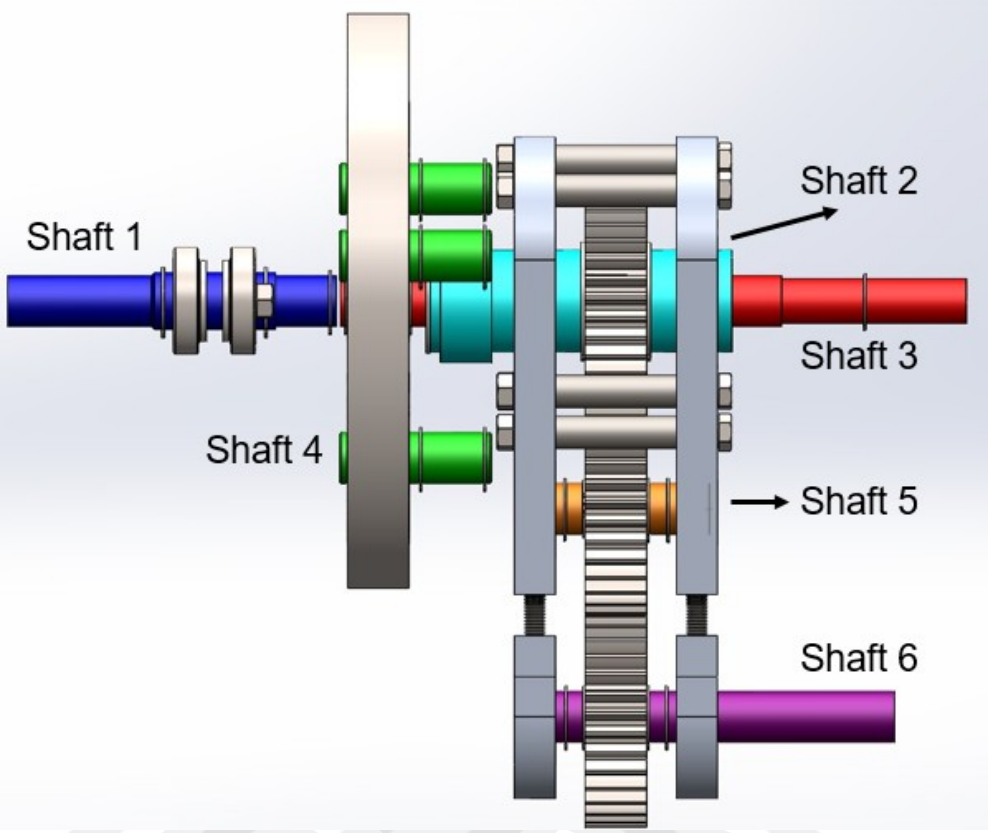

Figure 3.4 Gearbox Shaft Layout

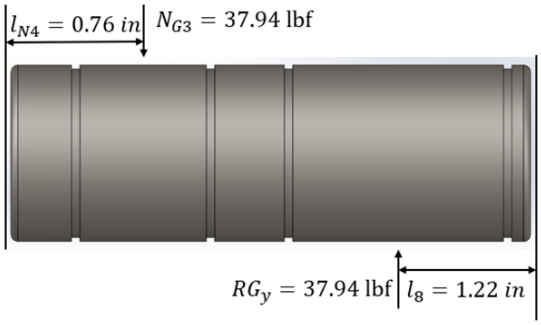

Figure 3.5 Free Body Diagram of Shaft #4.

is far above the 3 of the minimum safety factor, meaning these parameters are satisfactory for the safety of this design. The other shafts have higher safety factors, proving the safety of this design dictated by the application parameters of the design parameters.

Table 3.9 Load Parameter Constants of Shafts

Specification	**Values**
Bending Stress-Concentration Factor K_t	1.7
Bending Stress-Concentration Factor K_f	1.7
Torsional Stress-Concentration Factor K_{ts}	1.5
Torsional Stress-Concentration Factor K_{fs}	1.5
Marin Surface Modification Factor a	2.7
Marin Surface Modification Exponent b	-0.265
Loading Factor k_c	1
Temperature Factor k_d	1.02
Reliability Factor k_e	0.868

Table 3.10 Diameters, Stress and Safety Factors of Shafts

	Shaft 1	**Shaft 2**	**Shaft 3**	**Shaft 4**	**Shaft 5**	**Shaft 6**
Diameters	25mm	50mm, 4mm thickness	25mm	25mm	25mm	25mm
Alternating Stress σ_a	5.29 ksi	0 ksi	0 ksi	0.70 ksi	0.27 ksi	0.27 ksi
Midrange Stress σ_m	5.13 ksi	7.91 ksi	3.36 ksi	1.74 ksi	1.62 ksi	1.62 ksi
Safety Factor n_f	8.59	8.59	20.23	20.23	29.04	29.04

3.1.5. CAD Model

When the specifications for the mechanical parts found in the gearbox were finalized, the scaled drawing of a 3D model was done by using a 3D software, taking into account the dimensions required for this application and parts availability. Each part is modeled as per the ANSI-Metric standards and to scale. An example is given in the Figure 3.6.

After the parts were drawn, the assembly model was created on the same CAD software adding the ANSI-metric standard parts, such as gears or bearings. The carrier gear used for showing the calculation steps is given in the Figure 3.7.

After adding these standard parts, the assembly procedure was completed and each part was checked to ensure compatibility between parts and functionality. The 3D CAD model of the gearbox with isometric and side views are given in Figure 3.8.

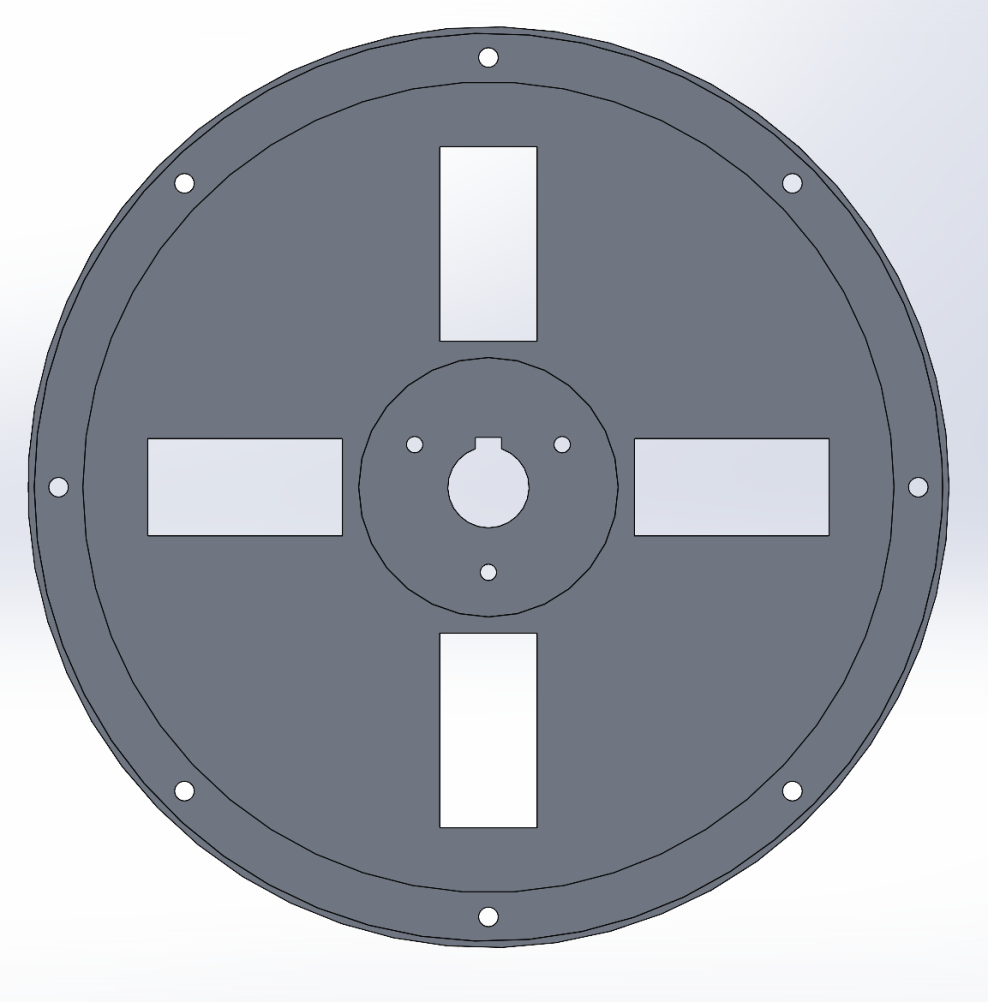

Figure 3.6 Front View of Ring Connector CAD Model.

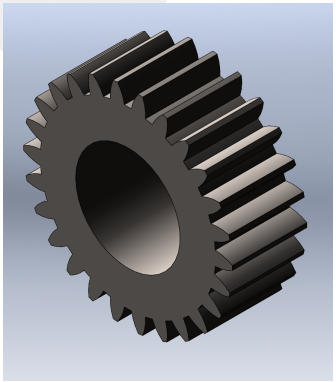

Figure 3.7 Isometric View of One of the Carrier Gears CAD Model.

3.1.6. Stress Analysis of Gearbox

The mechanical parts of the gearbox was tested using a commercial software. The key operating conditions, geometry, material and heat treatment, strength evaluations

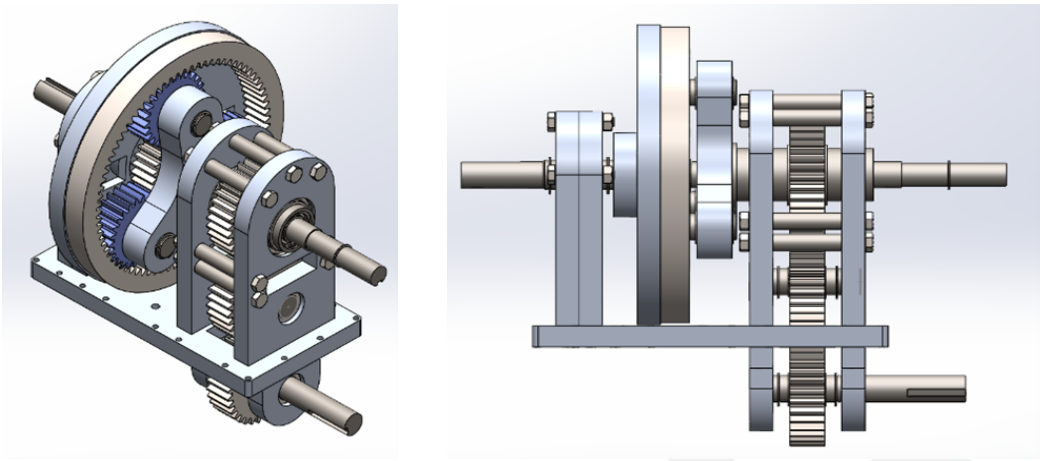

(a) Isometric (b) Side

Figure 3.8 Isometric and Side Cutaway Views of 3D CAD Model.

and service life of the sun, ring and carrier gears were analyzed and determined. The required service life was determined to be a minimum of 12000 hours, with the corresponding ISO standards taken for each measurement and calculation method. The key design parameters are given in the Table 3.11.

Table 3.11 Key Operating Parameters of the Gearbox

Parameter	**Value**
Input Power (kW)	30
Input Speed (RPM)	10000
Application Factor (KA)	2.5
Planet Carrier Speed (RPM)	2571
Circumferential Vel. (m/s)	31.5
Lubrication	ISO VG220 Oil

For this application due to the differences of the RPM in which the power units operate, a gear ratio is required and the following gear properties are chosen accordingly. Also, because of the given parameters above and a the minimum desired safety factor of 2.6 for n_c and 3.2 for n_b [20] is requested, 18CrNiMo7-6, a case-hardening steel known for high core toughness and surface hardness of about HRC 61 is chosen as the material for all gears. The Gear properties are presented in Table 3.12.

ISO 6336 is used to determine the strength of the gear, as it provides comprehensive calculation methods for the strength of the gear with contact stress / depression, tooth bending and service life factors [54]. For dynamic loads, ISO 6336-1 and for load spectrums, ISO 6336-2 are used. ISO 21171 is chosen as it is used for gear tooth

Table 3.12 Properties of Gears

Component	Teeth	Face width	Module	Pressure Angle
Sun Gear	27	17	3	20
Planetary Gear (x3)	26	17	3	20
Internal Ring Gear	78	17	3	20

geometry parameters, with consistent measurement and interchangeability. ISO 1328 is used for the profile and pitch accuracy grades for cylindrical gears. ISO/TS6336-20-21 is used for scuffing load capacity using integral and flash temperature methods, a crucial requirement for this application since the gears can spin as high as 10000 RPM.

Table 3.13 Tooth Root Stress Values of Gears

	Sun	Planet	Internal Ring
Nominal Stresss at Tooth Root (MPa)	13.54	13.51/12.46	11.11
Tooth Root Stress (MPa)	101.67	101.48/109.59	97.69
Permissible Tooth Root Stress (MPa)	495.77	362.06/359.20	506.10

Table 3.14 Contact Stress Values of Gears

	Sun-Planet	Planet-Internal Ring
Nominal Contact Stress (MPa)	248.40	131.27
Contact Stress at Operating Pitch Circle (MPa)	680.74	375.39
Contact Stress (MPa)	684.58/687.28	448.34/375.39

The calculations carried out by the software implicates that a safety factor of 2.9 at the minimum was achieved, which is within the design criteria and is consistent with the calcuations made above. In the table 3.15, the key safety factors for each gear are given.

Table 3.15 Safety Factors of Gears

	Sun	**Planet**	**Internal Ring**
Root Safety	9.865	7.966	
Root Safety		7.959	12.812
Flank Safety	2.909	3.065	
Flank Safety		4.897	5.848
Scuffing SF (Integral)	3.835	4.950	
Scuffing SF (Flash)	14.036	32,733	

As shown, the gears have a Root bending safety factors of 8 or above, significantly higher than the ISO minimum of 1.4. Flank pitting safety factors of 3 or above, which is higer than the ISO minimum of 1.0. Also, both integral and flash temperature Scuffing safety factors are above 3, indicating very low risk of scuffing.

The gearbox is shown to have a predicted service life of over 1 000 000 hours, which is far higher than the 12 000 hours reguired, with 100% reliability

The very high circumferential speed (31.5 m/s) requires careful lubrication planning. ISO VG 220 oil was selected to maintain adequate film thickness at elevated temperatures and speeds. Alternative synthetic oils with better thermal stability could further enhance performance.

Dynamic factor K_v reached the calculation limit, implying that vibration and resonance effects should be checked through experimental testing. Experimental testings of the gearbox show no NVH or resonance issues arise from sustained usage.

3.1.7. Manufacturing

After finalizing and freezing the CAD design of the gearbox, technical drawings of each one of the parts were created. After creating the technical drawings, parts were bought or manufactured according to the specifications. In the below figures, manufactured parts are shown. Each part was manufactured according to the ISO industry standard transition fit H7-k6 hole and K7-h6 shaft tolerance, allowing zero axial play and relatively easy assembly process, minimizing deformation and axial load risk.

Figure 3.9 Mechanical Parts for the Planetary Gearset

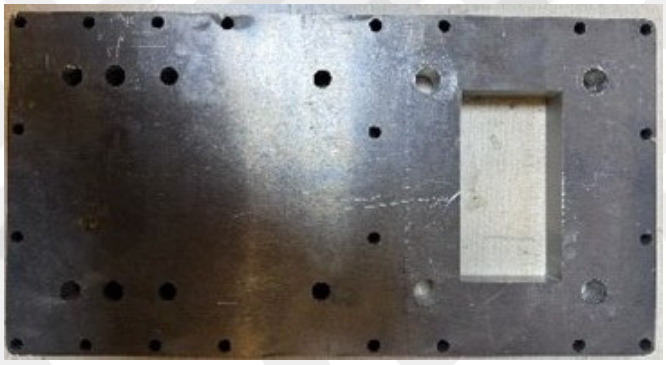

(a) Floor

(b) Shafts

Figure 3.10 Gearbox Mechanical Components

After buying or manufacturing the parts, the assembly procedure was conducted ac-

cording to the 3D CAD model. Certain small tweaks were made as necessary to migitate any production imperfections. The gearbox was tested at slow speeds for very short periods of time first to ensure the mechanism is working as intended. The assembled internals of the gearbox can be seen in the Figure 3.11

Figure 3.11 Mechanical Assembly for the Planetary Gearset

After ensuring the gearbox assembly is working as intended, the outer case, complete with an oil pan, was constructed to ensure the gearbox sits in a sealed and well-oiled closure to ensure minimal friction and maximum protection. The outer case construction is complete. The box with its case assembly in progress and completed can be seen in the figure 3.12.

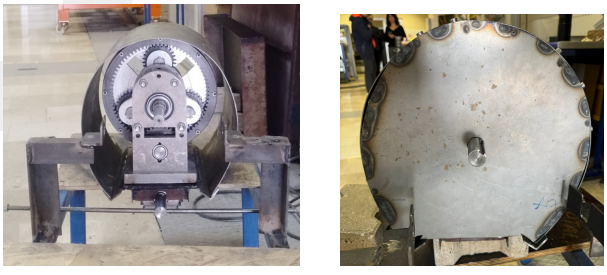

(a) In Progress (b) Complete

Figure 3.12 Gearbox Case Assembly

3.2. Hybrid Powertrain Modeling

As explained before, for hybridization, parallel hybrid was determined to be optimal for the requirements, with packaging, compatibility, cost and modularity constrains in mind. Parallel hybrids allow both power sources to independently power the traction wheels without any energy conversion required, reducing energy losses, complexity and cost since the existing engine and transmission, in theory, can be directly used [18]. Also, since the electric motor is only required to be a helping hand, a much smaller traction motor is sufficient, without any additional generators required [35].

3.2.1. Input Parameters

The 1/5 scaled passenger vehicle specifications were created according to the values presented in the table 3.17. For this application, a 2007 Yamaha YBR250 is chosen for the Combustion Engine (CE) and its gearbox. For all scenarios, the gear ratios are taken from the manufacturer specifications for the engine and transmission used as the CE side [55]. The gear ratios, along with the reduction ratios are given in table 3.16. For CE only traction, according to the speed and load, one of the available 5 speeds and its gear ratios were selected and used. When the gear ratios are calculated, for CE only traction, each gear gets its ratios multiplied by both the gearbox input and chain drive reduction ratios as both of them are used for providing positive traction to wheels. An equation is provided in eq.3.11 for calculating any of the gears total ratio. This method was used for calculating all five gear ratios for the CE only powertrain model. For Hybrid Traction, only one gear was selected since the CE is not used for low speed traction. Also, since the planetary gearbox is directly installed after the gearbox, the chain drive and gearbox input are removed, removing their reduction ratios. An equation is provided in eq.3.12 for calculating any gear in PHEV powertrain model. For each transmission used, its efficiency was taken as 97% according to literature research [49].

Table 3.16 Gear Ratios of the CE Gearbox

Gear/Reduction Type	**Gear Ratio**
Gearbox Input Reduction (i_{f1})	3.083
Chain Drive Reduction (i_{f2})	2.983
First Gear (i_1)	2.571
Second Gear (i_2)	1.684
Third Gear (i_3)	1.273
Fourth Gear (i_{r4})	1.040
Fifth Gear (i_{r5})	0.852

Table 3.17 Scaled Passenger Vehicle Model Parameters

Parameter	**Value**
Vehicle scale	1/5
Vehicle mass (kg)	200
Vehicle cross section (m^2)	0.7
Wheel diameter (cm)	50
Rotating mass ratio (%)	5
Rolling friction coefficient	0.008
Engine max Torque (N.m)	21 @ 5000 RPM
Engine max Power (kW)	15 @ 8000 RPM
Gasoline fuel density (kg/L)	0.745
Planetary Gearbox Ratio	2.89
EM max Torque (N.m)	14 @ 1500 RPM
EM max Power (kW)	2.2 @ 2200 RPM
Battery Nominal Voltage (V)	65
Battery Nominal Current (Ah)	15

$$i_{tot} = i_{f1} \times i_{f2} \times i_x \tag{3.11}$$

$$i_{tot} = i_x \tag{3.12}$$

For both equations, i_x is chosen according to the gear selected, for example i_1 is chosen for selecting first gear.

3.2.2. Simulation

The scaled prototype HEV model was created with the help of QSS-Toolbox, which makes it possible to design powertrain systems quickly and efficiently, while having flexibility to add or subtract components. Another advantage is that it is very easy to define the type of fuel to accurately define the fuel consumption and to define industry standard driving cycles, such as NEDC to test the powertrain according to the industry standards [56]. In Figure 3.13, the schematic view of the scaled vehicle models are presented. The first one, Figure (3.13a) is the conventional vehicle, with only the CE as the power unit. Its working condition is quasi state, meaning the vehicle is run on a driving cycle and the required torque and rotation is first calculated and then transferred to power sources. In a Parallel Hybrid Electric Vehicle (PHEV), shown on Figures 3.13b and 3.13c, there are two separate power sources. First is the CE, whose

fuel consumption is calculated in the 'Tank' subsystem. Second is the EM, whose energy capacity change in electric energy source is calculated in 'Battery' subsystem.

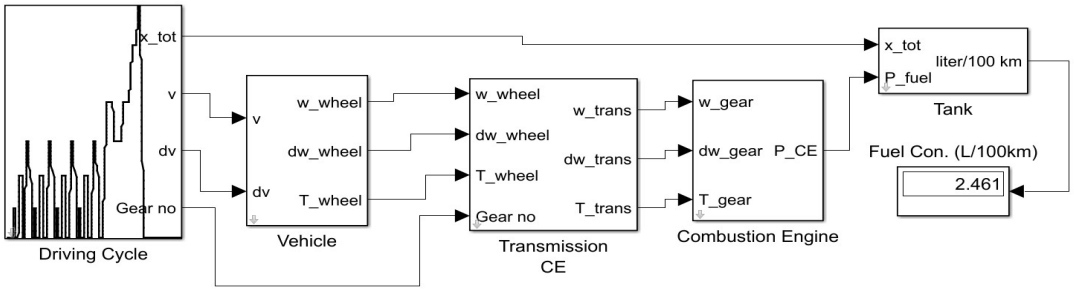

(a) CE Model

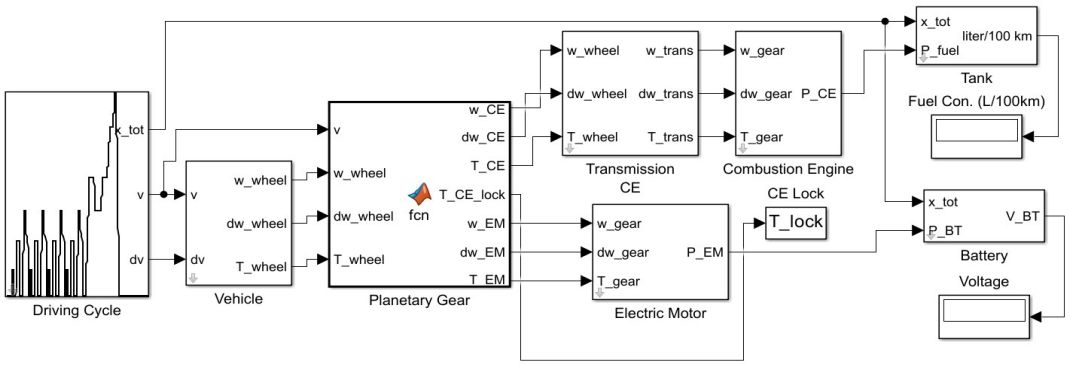

(b) PHEV Model with CE connected to Ring

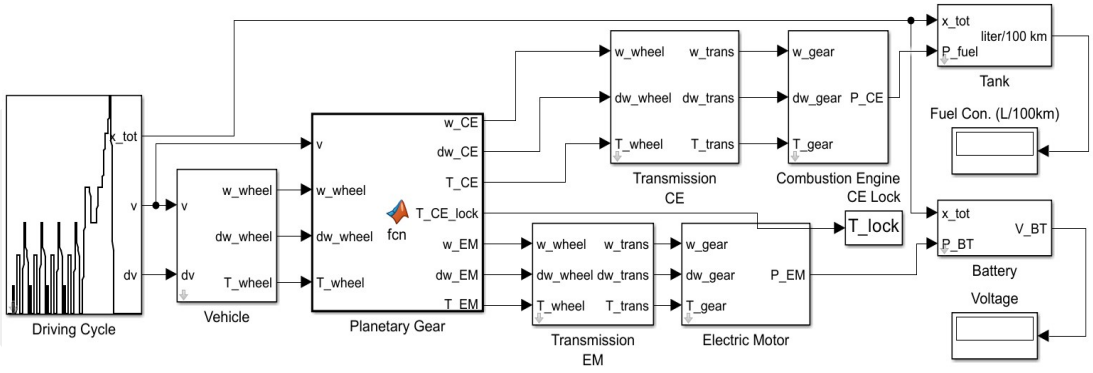

(c) PHEV Model with CE connected to Sun

Figure 3.13 Schematic view of CE and PHEV Vehicle Model

A planetary gearbox model is chosen as the speed coupler in PHEV model. The schematic view, along with the calculations are given in section 3.1.1. In this model, Part N.1 is the notation for the sun gear, Part N.2 is the notation for the ring gear and Part N.3 is the notation for the carrier gears. Two versions of this powertrain are created. In Figure 3.13b, the CE is connected to the ring gear and gear 5 is selected

($i_{CE} = 0.852$) while the EM is connected to the sun gear. In Figure 3.13c, the CE is connected to the sun gear and gear 1 is selected ($i_{CE} = 2.571$) while the EM is connected to the ring gear with a reduction gear ($i_{EM} = 3.1$) to match the speeds of EM and CE to enable operation.

CHAPTER 4

FINDINGS AND RESULTS

4.1. Electric Motor Efficiency Experimental Identification

To determine the efficiency of the gearbox on our hands, we need to determine the inertia caused by the dynamometer to ensure it is possible to accurately determine the efficiency of the gearbox. Several testing points were determined, ranging from 0-5 Nm torque and 100-2800 RPM, since the 2.2kW BLDC electric motor used for the benchmark testing can be effectively tested in between these parameters [48]. With testing points determined, the EM was tested without being connected to the dynamometer first to determine a base Torque and Power input values. Those values are given in Table 4.1.

Table 4.1 Power and Torque Values for the EM Only Case Study

Speed (RPM)	**Input Power(W)**	**Input Torque(Nm)**
100.00	33.71	3.22
200.00	36.36	1.74
300.00	42.30	1.35
400.00	48.25	1.15
500.00	54.12	1.03
600.00	61.38	0.98
700.00	68.54	0.93
800.00	75.13	0.90
900.00	83.69	0.89
1000.00	90.15	0.86
1100.00	100.02	0.87
1200.00	107.09	0.85
1300.00	114.14	0.84
1400.00	120.05	0.82
1500.00	130.35	0.83
1600.00	136.90	0.82
1700.00	146.50	0.82
1800.00	158.27	0.84
1900.00	172.39	0.87
2000.00	176.69	0.84
2100.00	180.60	0.82
2200.00	185.17	0.80
2300.00	191.39	0.79
2400.00	201.16	0.80
2500.00	206.05	0.79
2600.00	217.10	0.80
2700.00	223.26	0.79
2800.00	228.45	0.78

The same tests were repeated with the dynamometer connected to the EM without any external load applied to determine the moment and torque created from the dynamometer. Those results are given in the Table 4.2.

From these results, the torque applied from the dynamometer was calculated to be 0.5 Nm. With this information in hand, several load tests were conducted in different torque and RPM values to determine the efficiency of the electric motor under different loads to determine the efficiency map of the EM. The experiment results are given in the table below. Note that at some points, the experiment couldn't be carried out due to the power and torque limit of the EM. Those parts are denoted with an inf denotation.

Table 4.2 Power and Torque Values for the EM, Connected to Dyno Case Study

Speed (RPM)	**Input Power(W)**	**Input Torque(Nm)**	**$\triangle$ Pel (W)**
100.00	50.39	3.22	16.68
200.00	83.29	1.74	46.93
300.00	109.06	1.35	66.76
400.00	135.79	1.15	87.54
500.00	156.72	1.03	102.60
600.00	183.95	0.98	122.57
700.00	210.60	0.93	142.06
800.00	241.60	0.90	166.48
900.00	266.43	0.89	182.74
1000.00	293.21	0.86	203.06
1100.00	314.09	0.87	214.07
1200.00	343.14	0.85	236.05
1300.00	353.70	0.84	239.55
1400.00	366.71	0.82	246.66
1500.00	403.79	0.83	273.44
1600.00	431.12	0.82	294.22
1700.00	441.16	0.82	294.66
1800.00	470.32	0.84	312.06
1900.00	499.80	0.87	327.41
2000.00	529.57	0.84	352.88
2100.00	556.89	0.82	376.28
2200.00	584.62	0.80	399.46
2300.00	600.36	0.79	408.96
2400.00	617.14	0.80	415.98
2500.00	706.37	0.79	500.32
2600.00	733.13	0.80	516.03
2700.00	763.84	0.79	540.58
2800.00	858.20	0.78	629.75

From these efficiency values, the efficiency map of the EM was created as shown in the Figure 4.1.

Table 4.3 EM Efficiency (η_{em}) for Different Dyno Torque Values

Speed (RPM)	**0.5 Nm**	**1.0 Nm**	**1.5 Nm**	**2.0 Nm**	**3.0 Nm**	**4.0 Nm**	**5.0 Nm**
100.00	0.10	0.19	0.30	0.30	0.39	0.33	0.23
200.00	0.13	0.24	0.32	0.36	0.50	0.42	0.32
300.00	0.14	0.26	0.35	0.41	0.54	0.44	0.34
400.00	0.15	0.28	0.37	0.44	0.55	0.45	0.38
500.00	0.17	0.29	0.37	0.47	0.55	0.48	0.38
600.00	0.17	0.29	0.38	0.46	0.63	0.50	0.39
700.00	0.17	0.31	0.36	0.47	0.62	0.50	0.41
800.00	0.17	0.31	0.37	0.48	0.65	0.51	0.42
900.00	0.18	0.32	0.39	0.49	0.65	0.52	0.43
1000.00	0.18	0.31	0.41	0.51	0.65	0.55	0.42
1100.00	0.18	0.33	0.41	0.52	0.61	0.54	0.44
1200.00	0.18	0.33	0.43	0.53	0.63	0.54	0.44
1300.00	0.19	0.34	0.43	0.53	0.65	0.55	inf
1400.00	0.20	0.34	0.44	0.55	0.65	0.55	inf
1500.00	0.19	0.34	0.44	0.56	0.67	0.55	inf
1600.00	0.19	0.35	0.44	0.57	0.68	inf	inf
1700.00	0.20	0.35	0.45	0.58	0.67	inf	inf
1800.00	0.20	0.35	0.44	0.57	0.70	inf	inf
1900.00	0.20	0.35	0.42	0.54	0.71	inf	inf
2000.00	0.20	0.36	0.43	0.55	inf	inf	inf
2100.00	0.20	0.37	0.45	0.56	inf	inf	inf
2200.00	0.20	0.37	0.47	0.57	inf	inf	inf
2300.00	0.20	0.38	0.47	0.58	inf	inf	inf
2400.00	0.20	0.37	0.48	0.58	inf	inf	inf
2500.00	0.19	0.35	0.30	0.59	inf	inf	inf
2600.00	0.19	0.35	0.49	inf	inf	inf	inf
2700.00	0.18	0.36	0.50	inf	inf	inf	inf
2800.00	0.17	0.35	0.49	inf	inf	inf	inf

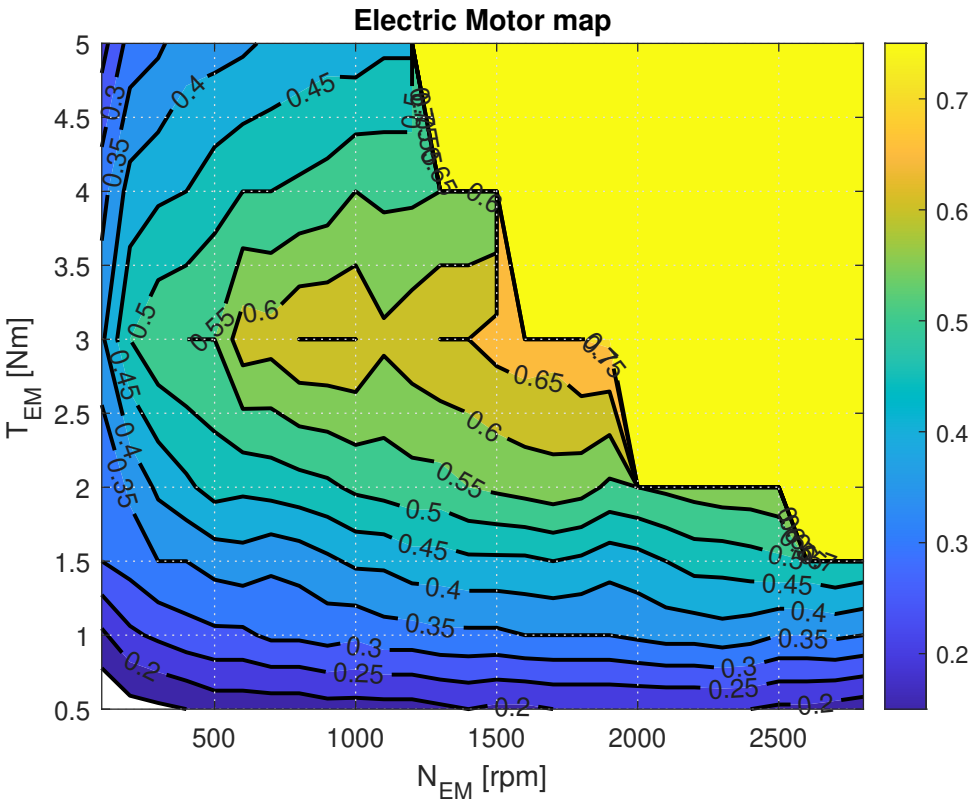

Figure 4.1 Efficiency Map for the EM

With the efficiency map of the EM known, it is possible to accurately test the efficiency of the gearbox in different testing points. For this test, the gearbox is required to be connected between the EM and the dynamometer. The gearbox is connected to the dynamometer and the EM is connected to the gearbox in both inputs to determine the efficiency of the gearbox in both input shafts.

4.2. Gearbox Reduction Ratio Experimental Measurement

Recalling from section 3.1, in order to determine the gear ratios between the sun, carrier and ring gears, i_g is required. Recalling the equation 3.6, R_s and R_r the radius of sun gear and ring gear respectively, or Z_s and Z_r, tooth number of sun gear and ring gear respectively, are needed. For this application, the tooth numbers or sun and ring gears are taken as $Z_s = 27$ and $Z_r = 78$, respectively, due to the operational RPM range difference between the ICE and EM chosen for this application. Inserting them into 3.6 gives the following result

$$i_g = i_{1-2}^3 = \frac{Z_r}{Z_s} = \frac{78}{27} = 2.89 \tag{4.1}$$

With $i_g = 2.89$, the gear ratios between the sun, carrier and ring gears can be determined by using the equation below and fixing one of the ends to reduce the the unknown values for the equation.

$$w_c = \frac{1}{1+i_g} w_s = \frac{i_g}{1+i_g} w_r \tag{4.2}$$

In the Figure 4.2, port numbers are labeled on the planetary gearbox in which P_1 is the ICE input, which is connected to the ring gear, P_2 is the EM input, connected to the sun gear, and P_3 is the output, connected to the carrier gears, or yoke. The reason for this port number is for gear ratios(expand)

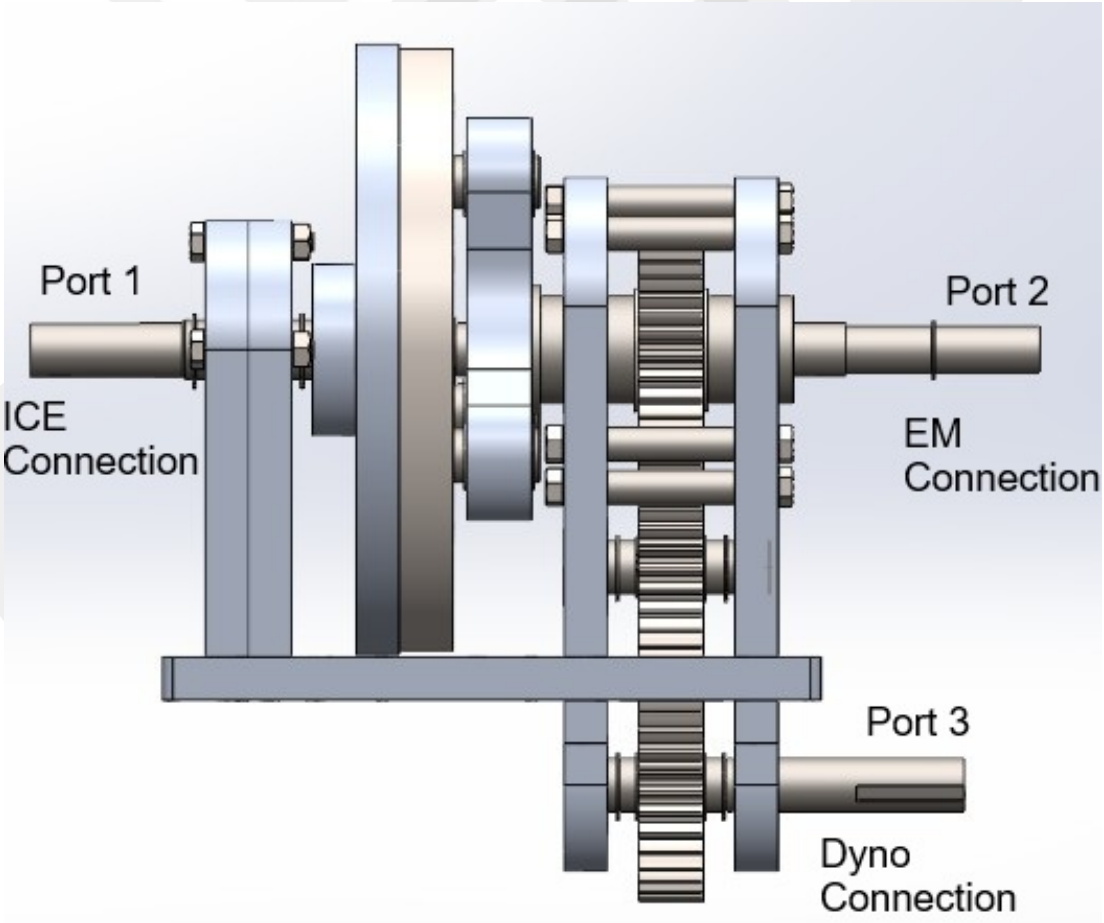

Figure 4.2 Planetary Gearbox Port Connections

4.2.1. Gear Ratio Measurement of P_2 to P_3 Power Line

In this testing scenario, the EM is connected to the P_2 port and the P_1 port is fixed, meaning the ring gear is fixed, meaning $w_r = 0$. With $i_g = 2.89$, the 3.8 can be rearranged to determine the gear ratio between P_2 and P_3

$$w_c = \frac{1}{1+2.89} w_s = \frac{1}{3.89} w_s \tag{4.3}$$

With this relation, it can be determined that the gear ratio between P_2 and P_3 is 3.89, meaning for every rotation in P_3, 3.89 rotations will be made in P_2..

In Figure 4.3, the measured speeds in P_2 (EM) and P_3 (Dyno) ports are given. For the speed measurement, a tachometer was used on both ends, the data was captured and filtered before being plotted in MATLAB. Both the raw and filtered data are shown. Legends for each line are given.

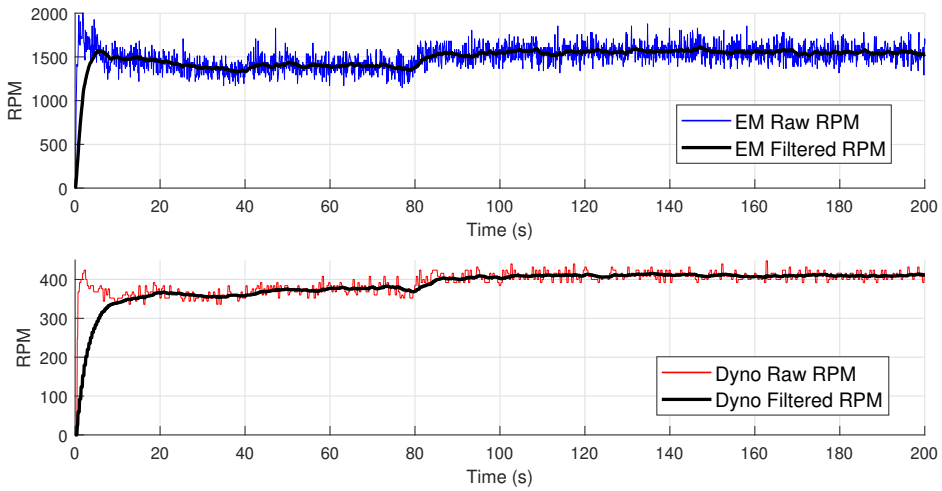

Figure 4.3 Measured Speeds in P2 and P3 Ports

4.2.2. Gear Ratio Measurement of P_1 to P_3 Power Line

In this testing scenario, the EM is connected to the P_1 port and the P_2 port is fixed, meaning the sun gear is fixed, meaning $w_s = 0$. With $i_g = 2.89$, the 3.8 can be rearranged to determine the gear ratio between P_1 and P_3

$$w_c = \frac{2.89}{1 + 2.89} w_r = \frac{1}{1.35} w_r \tag{4.4}$$

With this relation, it can be determined that the gear ratio between P_1 and P_3 is 1.35, meaning for every rotation in P_3, 1.35 rotations will be made in P_1.

In Figure 4.4, the measured speeds in P_1 (EM) and P_3 (Dyno) ports are given. As before, for the speed measurement, a tachometer was used on both ends, the data was captured and filtered before being plotted in MATLAB. Both the raw and filtered data are shown. Legends for each line are given.

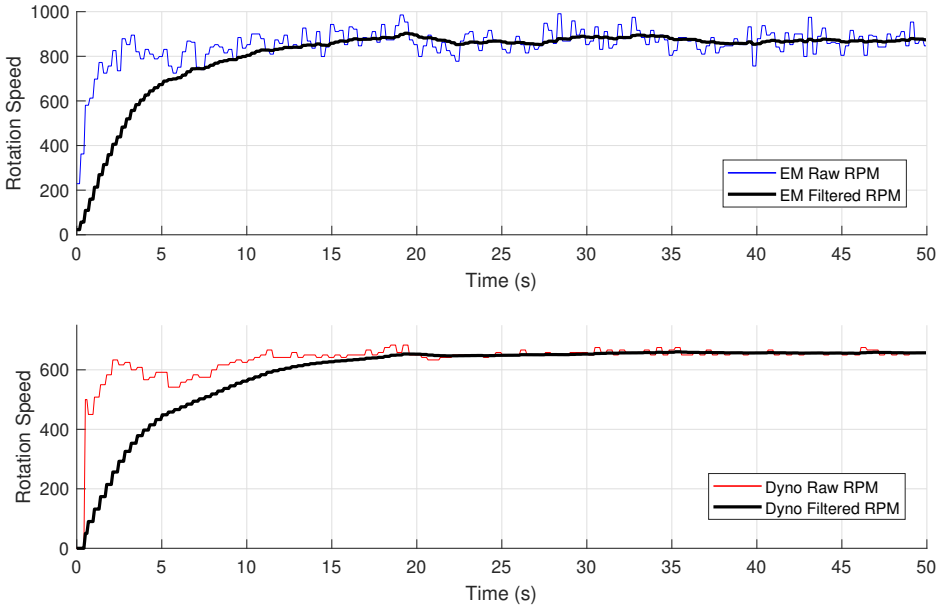

Figure 4.4 Measured Speeds in P1 and P3 Ports

4.3. Gearbox Efficiency Experimental Measurement

To determine the efficiency (η) of the gearbox, the total efficiency of the system needs to be determined first. An easy way to determine η is to measure the mechanical power, P_m, and divide it with power input, P_{in}.

$$\eta = \frac{P_m}{P_{in}} \tag{4.5}$$

The P_m can be determined with the applied torque (T_m), which can be adjusted and determined from the dynamometer and the rotational velocity (w_m) which can me measured from the tachometer, using the following relation

$$P_m = T_m \times w_m \tag{4.6}$$

Similarly, the input power can be determined as

$$P_in = T_in \times w_{in} \tag{4.7}$$

In an EM application, knowing the voltage (V_{in}) and current (A_{in}), with the following relation, the electric power input (Pe) can be determined as

$$P_e = V_{in} \times A_{in} \tag{4.8}$$

For the power output of the electric motor, the efficiency of the electric motor is required. In section 4.1, the efficiency of the EM (η_{em}) was determined across several points. Using those data, the power output of the EM can be determined as follows

$$P_{em} = P_e \times \eta_{em} \tag{4.9}$$

Combine the equations 4.5 and 4.8 for the total efficiency for the testing measurements to be as follows

$$\eta_{tot} = \frac{P_m}{P_e} \tag{4.10}$$

And combining equations 4.9 with 4.10, the gearbox efficiency can be determined as follows

$$\eta_{GB} = \frac{P_m}{P_{em}} \tag{4.11}$$

4.3.1. Efficiency Measurement of P_2 to P_3 Power Line

To determine the efficiency of the gearbox in the power flow direction P_2 and P_3, a testing scenario was devised. The EM was to be driven at wide open throttle and the torque applied from the dynamometer was to be changed every 20 seconds, from $T_m = 0Nm$ to $T_m = 7Nm$, at $1Nm$ increments. During the test, the power input at the P_2 port and the power output at the P_3 is required to be measured or calculated. To determine the power input at P_2 port, the T_{em}, w_{em}, P_e and $P_{em} = P_2$ are required. First, T_{em} and w_{em} values can be determined from figure 4.5. Second, by taking the V_{in} and A_{in} values from Figure 4.6, P_e can be calculated using the Equation4.8 Third, recalling the EM efficiency values from sec. 4.1, taking the P_e calculated and using the Equation 4.9, power input (P_2) can be determined. To determine the power output at the P_3 port, w_m, T_m are required to determine $P_m = P_3$. The values w_m and T_m can be determined from Figure 4.5, and then inserted into Equation 4.6.

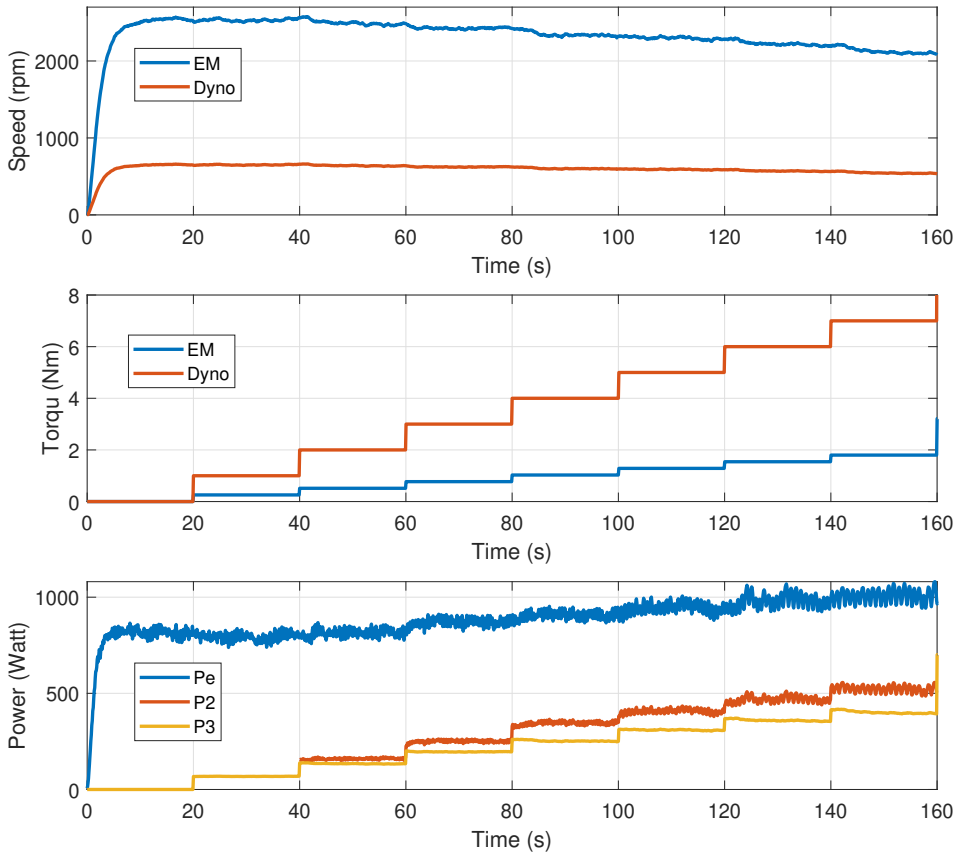

Figure 4.5 Measurement EM Parameters for Power Input (P_2) and Output (P_3) in Gearbox Efficiency Testing

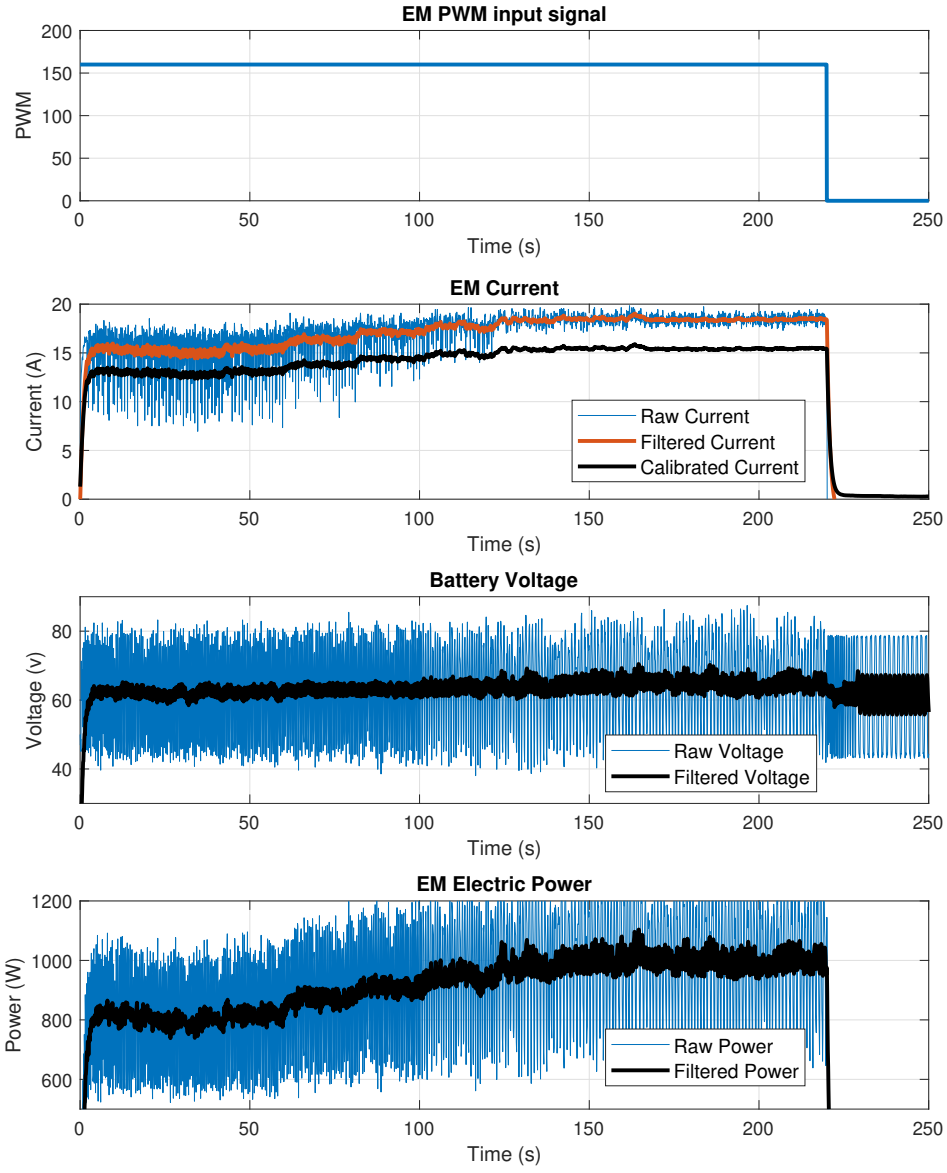

Figure 4.6 Measurement Battery Parameters for Power Input (P_2) and Output (P_3) in Gearbox Efficiency Testing

From the values extracted from Figures 4.5 and 4.6, the power input at the P_2 port and the power output at the P_3 are calculated, along with the EM power input (P_e). With these power values, the efficiency of the system can be determined with eq. 4.10 and the efficiency of the gearbox can be determined with eq.4.11 In Figure 4.7, the EM, gearbox and total efficiencies are displayed. The average gearbox efficiency is determined to be about 80% in this power line. There are two main reasons for the relatively low efficiency in this power line when compared to commercial applications. First, the manufacturing and assembly tolerance limitations which are the results of limited budget and facilities are a main culprit since the assembly has some unwanted tolerance values related to the limitations explained above. Second, related to the issue above as well, is the limited oiling capacity of the gearbox since it only sits in an oil bath without any oil pumps or oil jets to properly lubricate the mechanical parts of the gearbox.

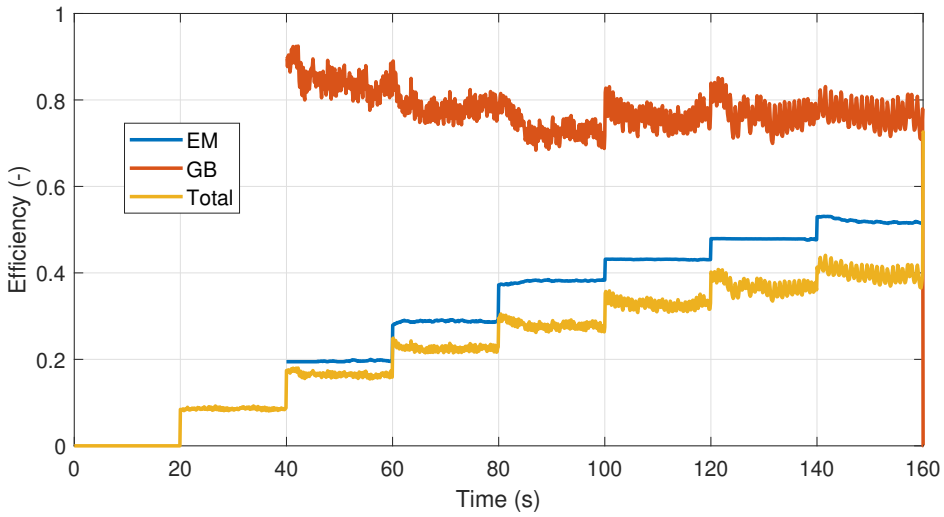

Figure 4.7 GB Efficiency in P_2 to P_3 Power Line

From Figure 4.7, the efficiencies can be seen. The efficiency of which the EM is operating relative to its efficiency map during this testing period can be seen clearly in Figure 4.8.

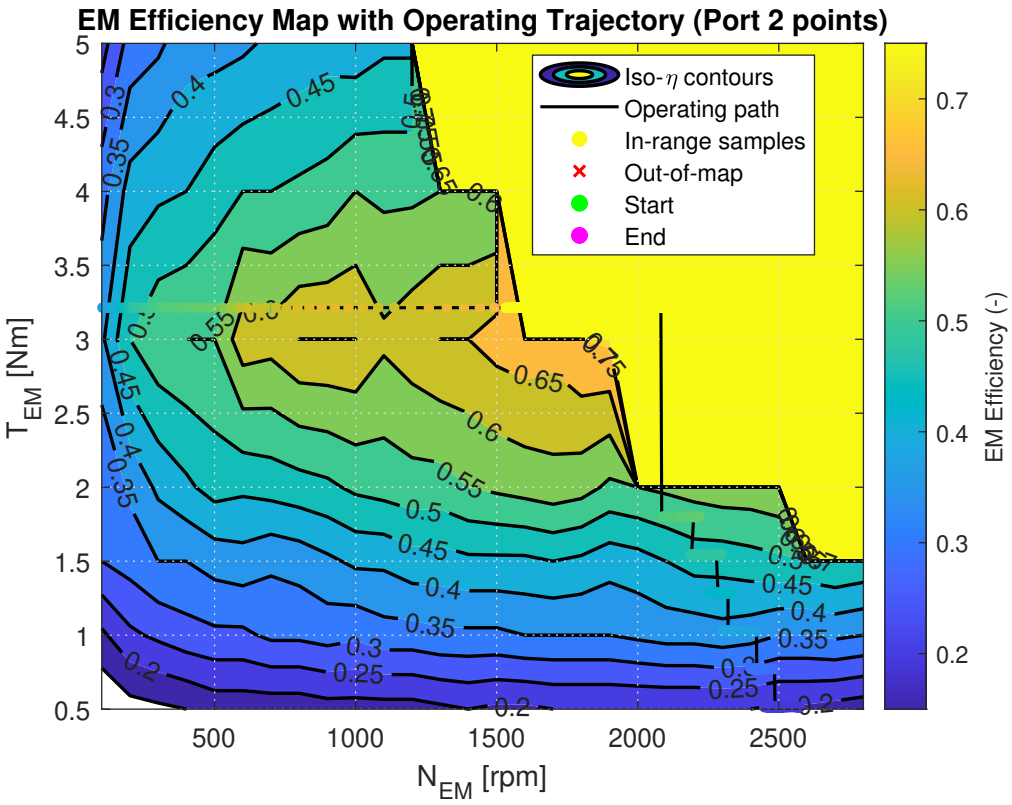

Figure 4.8 EM Efficiency Map with Operation Points in P_2 to P_3 Power Line

4.3.2. Efficiency Measurement of P_1 to P_3 Power Line

To determine the efficiency of the gearbox in the power flow direction P_1 and P_3, a testing scenario was devised. The EM was to be driven at wide open throttle and the torque applied from the dynamometer was to be changed every 20 seconds, from $T_m = 0Nm$ to $T_m = 7Nm$, at $1Nm$ increments. During the test, the power input at the P_1 port and the power output at the P_3 is required to be measured or calculated. To determine the power input at P_1 port, the T_{em}, w_{em}, P_e and $P_{em} = P_1$ are required. First, T_{em} and w_{em} values can be determined from figure 4.9. Second, by taking the V_{in} and A_{in} values from figure 4.10, P_e can be calculated using the equation4.8. Third, recalling the EM efficiency values from sec. 4.1, taking the P_e calculated and using the equation 4.9, power input (P_1) can be determined. To determine the power output at the P_3 port, w_m, T_m are required to determine $P_m = P_3$. The values w_m and T_m can be determined from Figure 4.9, and then inserted into Equation 4.9

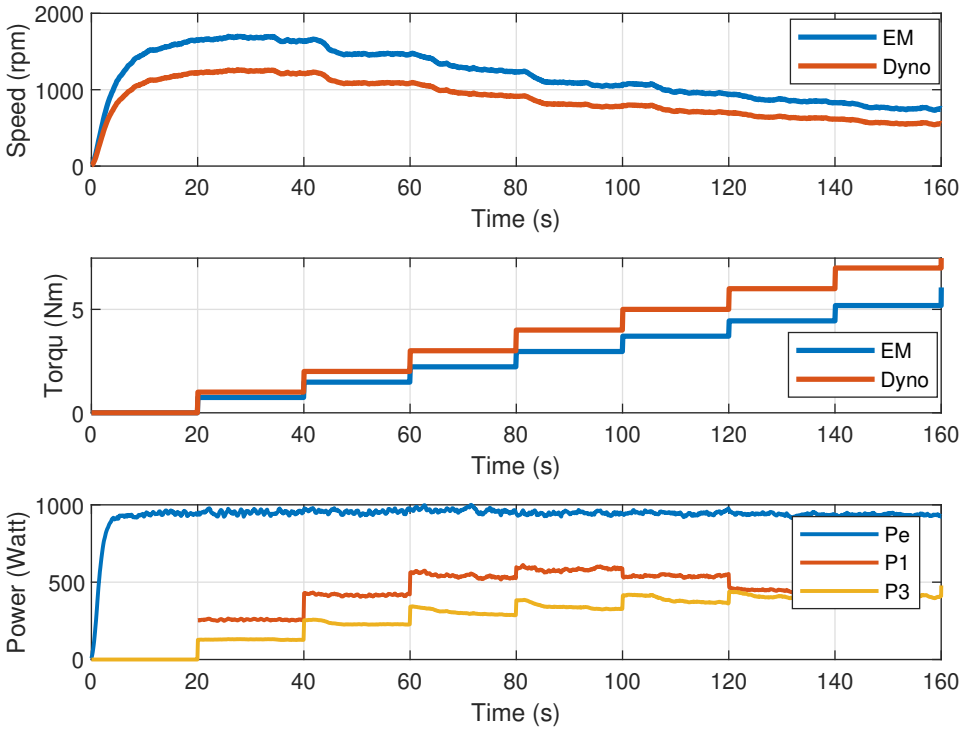

Figure 4.9 Measurement EM Parameters for Power Input (P_2) and Output (P_3) in Gearbox Efficiency Testing

From the values extracted from Figures 4.9 and 4.10, the power input at the P_1 port and the power output at the P_3 are calculated, along with the EM power input (P_e). With these power values, the efficiency of the system can be determined with eq. 4.10 and the efficiency of the gearbox can be determined with Equation 4.11 In Figure 4.11, the EM, gearbox and total efficiencies are displayed. The average gearbox efficiency is determined to be about 60% in this power line. There are three main reasons for the relatively low efficiency in this power line when compared to commercial applications. First, the manufacturing and assembly tolerance limitations which are the results of limited budget and facilities are a main culprit since the assembly has some unwanted tolerance values related to the limitations explained above. Second, related to the issue above as well, is the limited oiling capacity of the gearbox since it only sits in an oil bath without any oil pumps or oil jets to properly lubricate the mechanical parts of the gearbox. Third reason for the lower efficiency in this power line is the nature of planetary gearbox systems since they generally have higher efficiency on the sun-carrier power line when compared to ring-carrier power line.

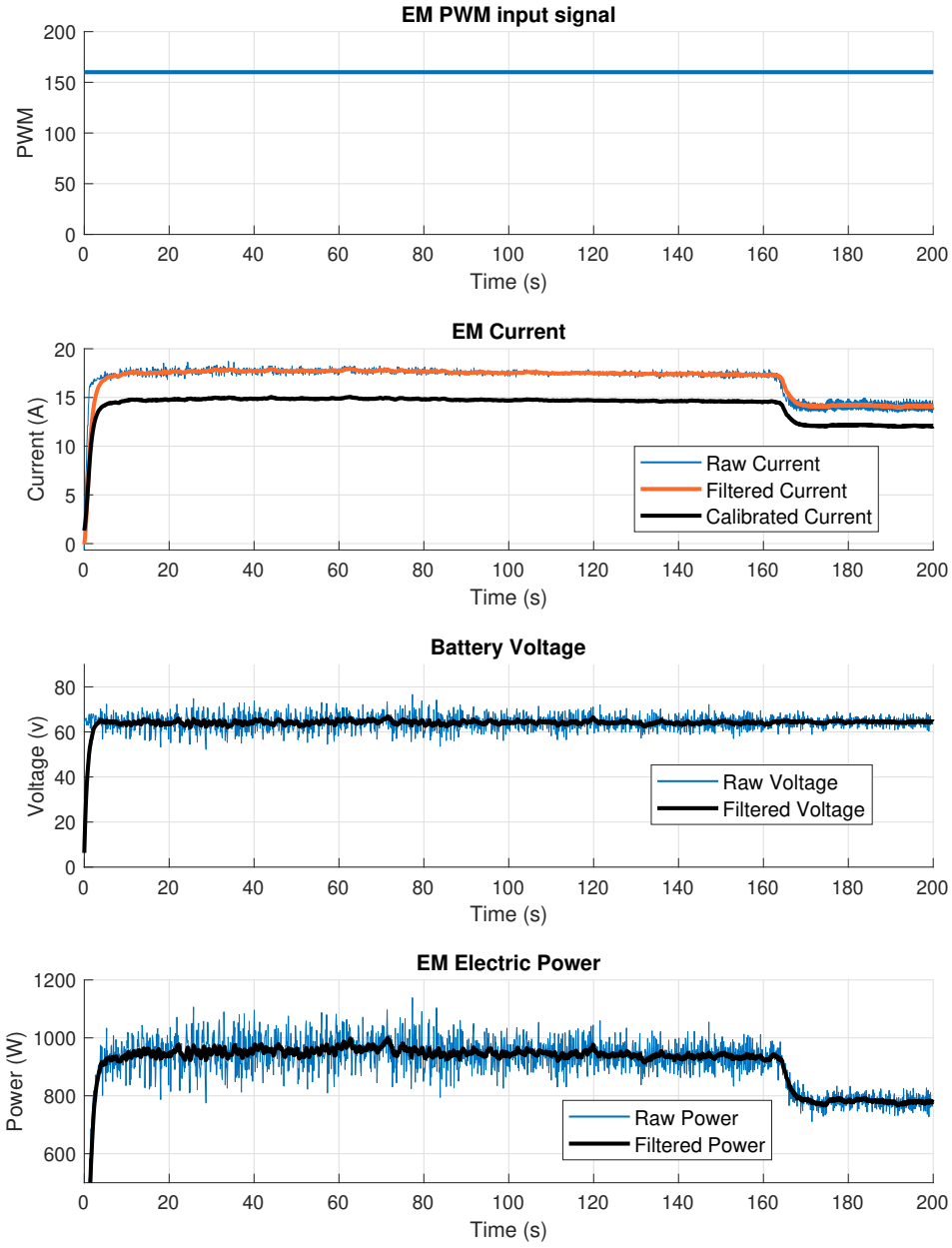

Figure 4.10 Measurement Battery Parameters for Power Input (P_2) and Output (P_3) in Gearbox Efficiency Testing

From Figure 4.11, the efficiencies can be seen. The efficiency of which the EM is operating relative to its efficiency map during this test can be seen in Figure 4.12.

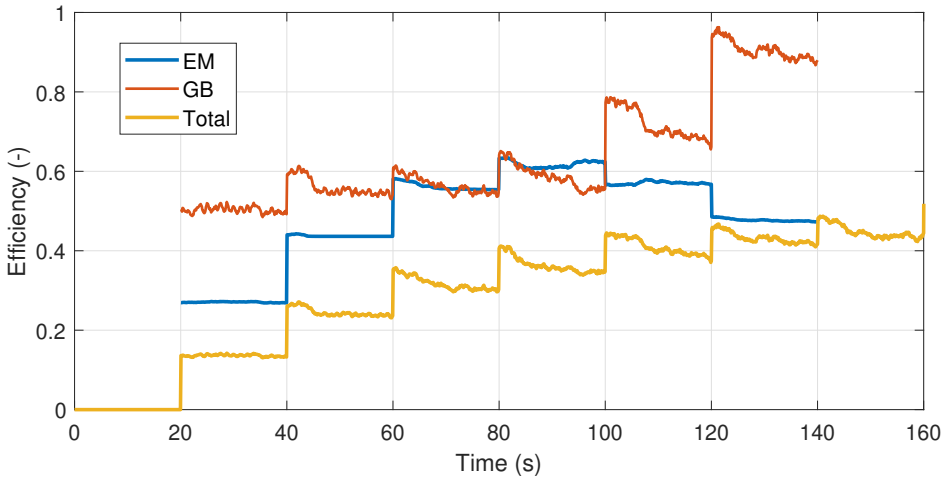

Figure 4.11 GB Efficiency in P_1 to P_3 Power Line

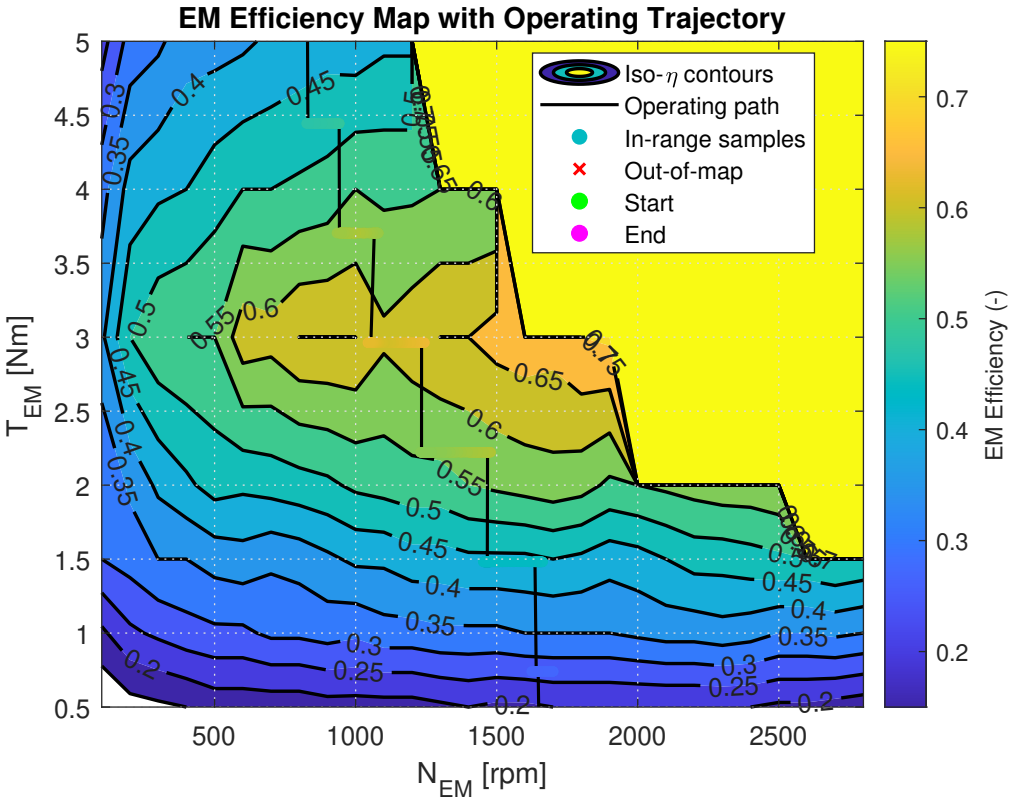

Figure 4.12 EM Efficiency Map with Operation Points in P_1 to P_3 Power Line

4.4. Hybrid Powertrain Simulation Results

The scaled model was run on an NEDC urban driving cycle since the advantage of the PHEV powertrain design can be shown in urban driving scenarios. For comparing the powertrains between conventional CE and PHEV designs, NEDC driving cycle was chosen for its industrial standard application. In Figure 4.13, the velocity of the vehicle is given and using the integration of velocity data, the distance traveled was calculated to be 10.92 km.

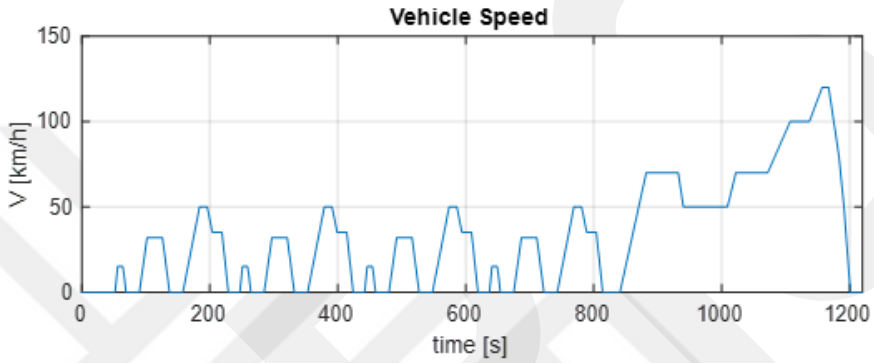

Figure 4.13 Velocity Data for NEDC Driving Cycle

With the rolling and aerodynamic resistances, along with acceleration forces, the requested traction power on wheels are calculated and can be found in Figure 4.14

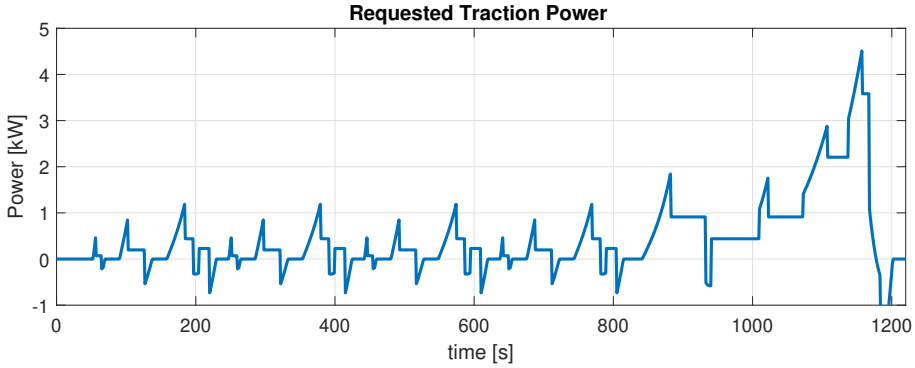

Figure 4.14 The Requested Traction Power on Vehicle Wheels Running on NEDC

In order to provide this requested power by wheels, for the conventional vehicle, CE has been utilized while in PHEVs both the CE and EM were utilized. Figures 4.15 and 4.16 highlights the different power sharing between three different powertrain configurations. In Figure 4.15, only CE power has been used to deliver requested power.

The power curve of the CE is always above the requested traction power, power line efficiency being the main reason. Negative wheel power is deceleration power, which can't be harvested by CE and instead converted to heat loss using the available mechanical braking system.

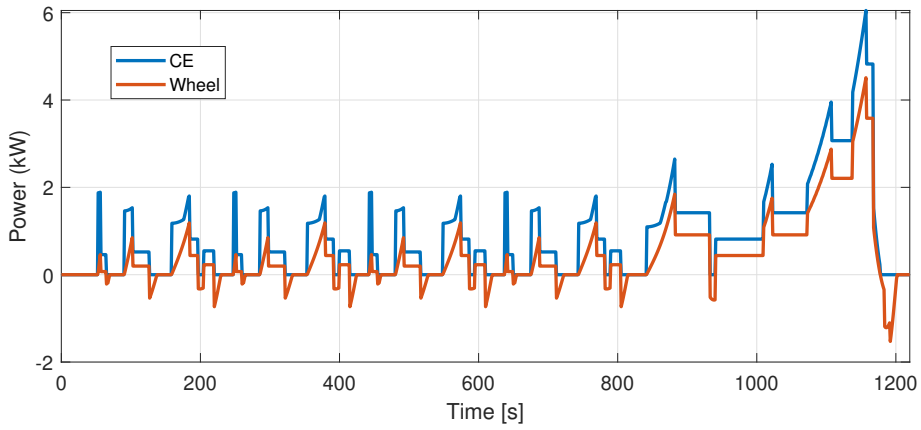

Figure 4.15 Power Sharing in Conventional Design Running on NEDC

In Figure 4.16, EM power, as well as CE power has been used to deliver requested power. A simple power sharing control strategy has been devised in which at low speeds (below 49 km/h for CE connected to Ring in Figure 4.16a and 33 km/h for CE connected to Sun in Figure 4.16b), the EM is being utilized only. At high speeds (above 49 km/h for CE connected to Ring and 33 km/h for CE connected to Sun), the CE is used with EM. The total power curve on hand is always above the requested traction power, power line efficiency being the main reason. Negative wheel power is deceleration power, which can be harvested by EM and can be stored in the battery pack for later use.

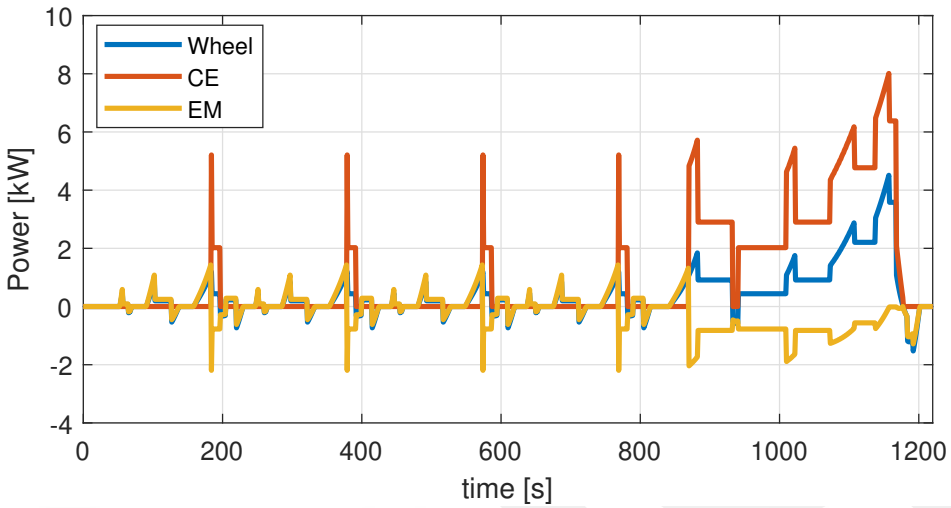

(a) CE connected to Ring Gear

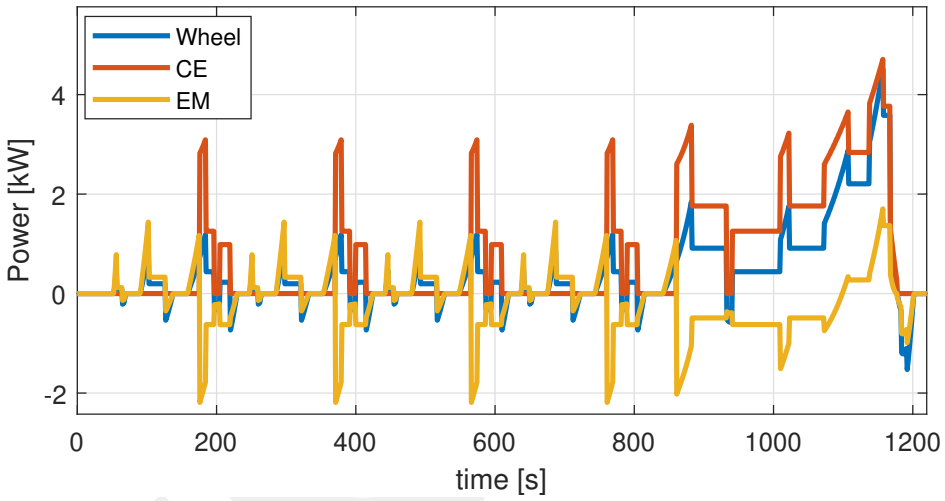

(b) CE connected to Sun Gear

Figure 4.16 Power Sharing in Different Designs Running on NEDC

In the Figure 4.17, the CE operation points for conventional design is shown. In Figure 4.18, CE operation points for both PHEV applications are shown. Note that CE is the primary power design for all applications. As the CE is naturally the only power source in the conventional powertrain, every power request is supplied by the CE. Although it has a gearbox with 5 speeds to aid in operating at relatively efficient regions, this still results in the CE operating at different regions, including low efficiency points. The results of the CE operation points is shown in 4.17, and the gear ratios, along with chosen gear at each point is shown in Figure 4.18.

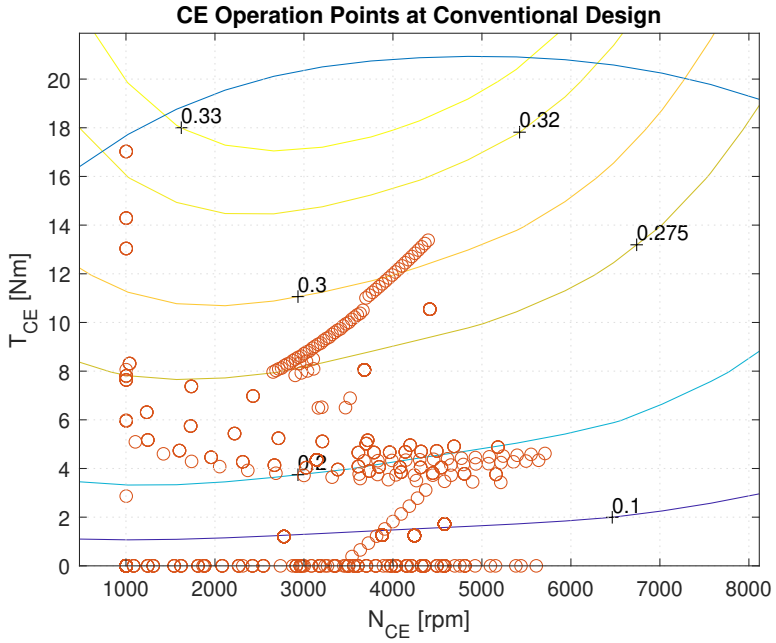

Figure 4.17 CE Operation Points in Conventional Design Running on NEDC

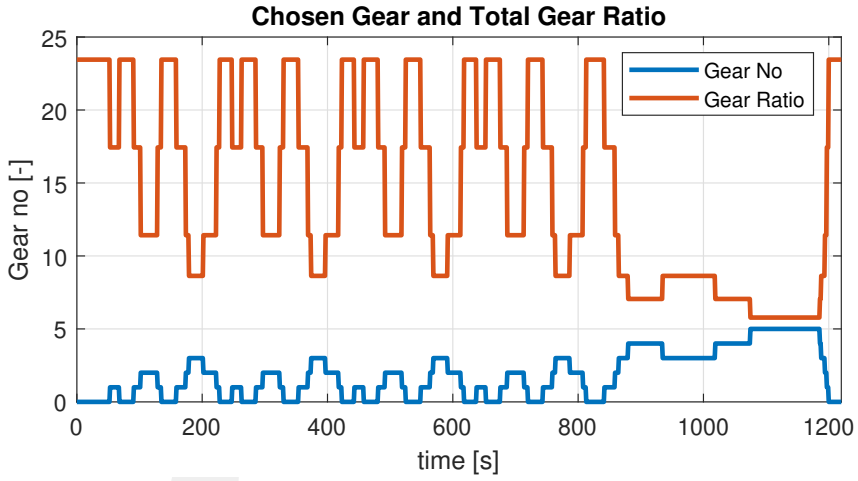

Figure 4.18 Gear Operation Points in Conventional Design Running on NEDC

For the PHEV Powertrains, the result is considerably different, as shown in Figure 4.19. Here, the CE is in operation with EM, which acts as the assistant of CE. This eliminates the need to use CE for all power requests, allowing the CE to be operated at high efficiency regions only. For this application, according to the control strategy, the constant speed of $\approx$ 4400 rpm for ICE connected to ring gear and $\approx$ 3200 rpm for ICE connected to sun gear and moderate torque values have been determined for both architectures. With a planetary gearbox, speed summation can be achieved in a PHEV

setup. This allows the CE to be used at a set RPM, increasing its efficiency, while the EM can be used at variable speeds. With this method, it is possible to concentrate the CE to operate at its high efficiency region, which is the first advantage presented by this method.

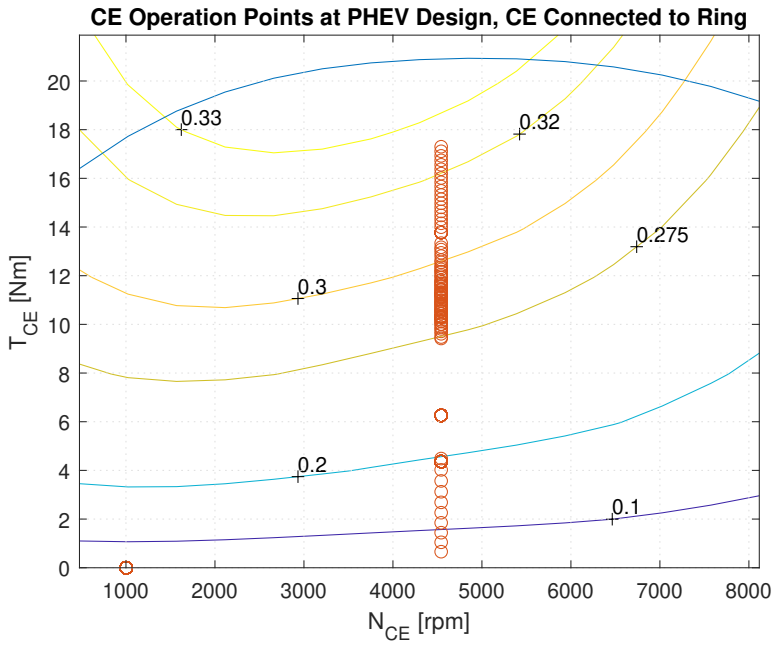

(a) CE connected to Ring Gear

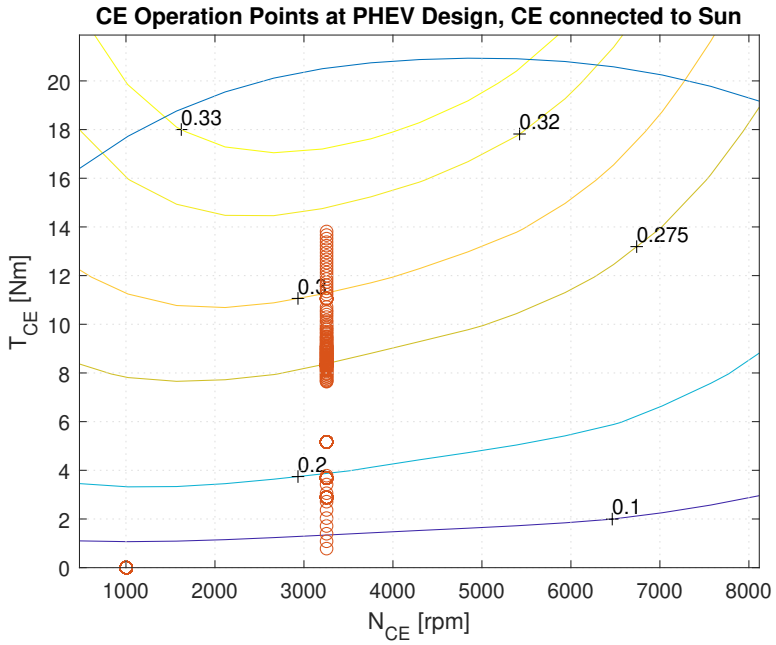

(b) CE connected to Sun Gear

Figure 4.19 CE Operation Points in Different PHEV Designs Running on NEDC

The Figures 4.20 and 4.21 displays the operation points of EM in both PHEV designs, with Figure 4.20 showing the EM connected to sun gear and Figure 4.21 showing the EM connected to ring gear. Efficiency contours along with the circles, denoting the operation points, prove a clear condition of EM in this application. The map was extended in both positive and negative directions of T_{em} and w_{em}. The map can be divided to 4 regions. The region with positive T_{em} and w_{em} represents the Hybrid Traction mode, negative T_{em} and positive w_{em} represents the regenerative braking mode, where part of the deceleration power is captured and stored for later use, reducing losses such as heat losses due to using mechanical brakes. NegativeT_{em} and w_{em} represent the region in which the EM acts as a generator, powered by CE. Also to note that negative w_{em} means the rotation is in the opposite direction.

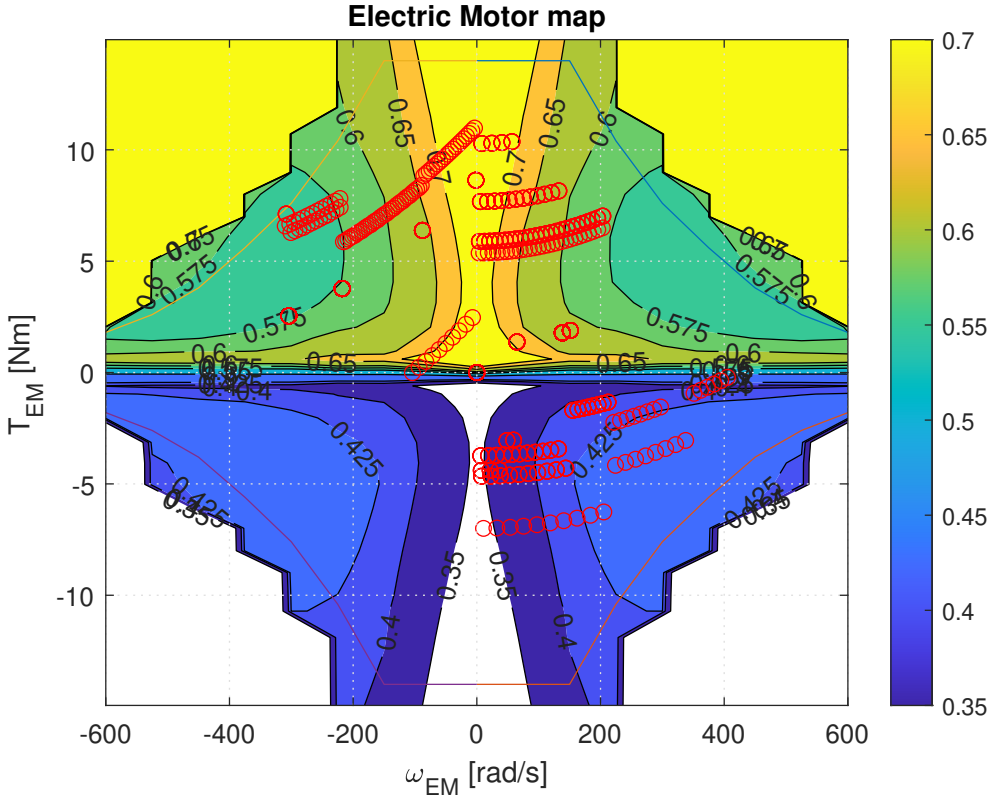

Figure 4.20 EM Operation Points of EM Connected to Sun Gear in PHEV Design Running on NEDC

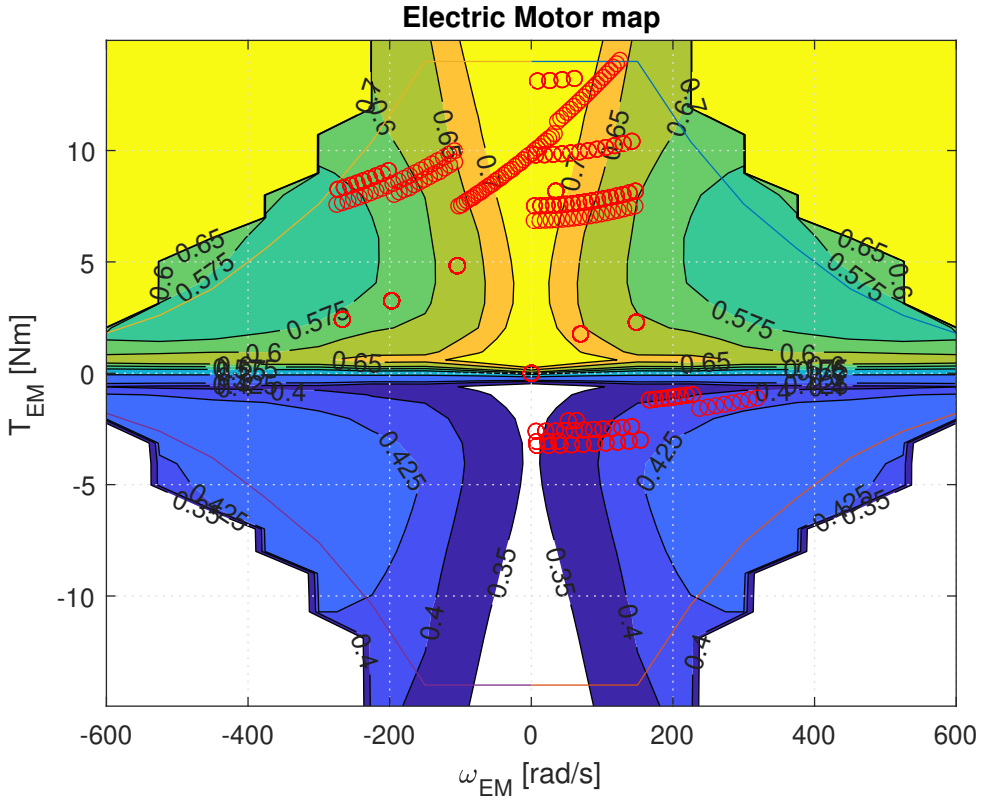

Figure 4.21 EM Operation Points of EM Connected to Ring Gear in PHEV Design Running on NEDC

The Figures 4.22 and 4.23 shows the variation present in battery states in the PHEV powertrains, with Figure 4.22 showing the EM connected to sun gear and Figure 4.23 showing the EM connected to ring gear, tested on NEDC duty cycle. Battery charge ratio curve, also known as State of Charge (SoC) curve here displays the battery was discharged first up to around two-thirds of the cycle, with the local increases accounting for the energy required during regenerative braking. For the remaining one third part of the driving cycle, the SoC curve shows an increase until the initial SoC value is obtained for both architectures. This is the result of the CE being used both as a propulsion unit and as a generator, thanks to the planetary gearbox coupling. Battery voltage curve shows that the nominal battery voltage is shown to be around 60v, increasing or decreasing according to the charging or discharging of the battery pack. Battery current curve displays the different points on which there are instantaneous loads on the battery, along with their amount. The last curve, battery power, displays the instantaneous power flow to the battery, having a positive value when the battery is delivering power to the EM and negative when the battery is charged by the EM.

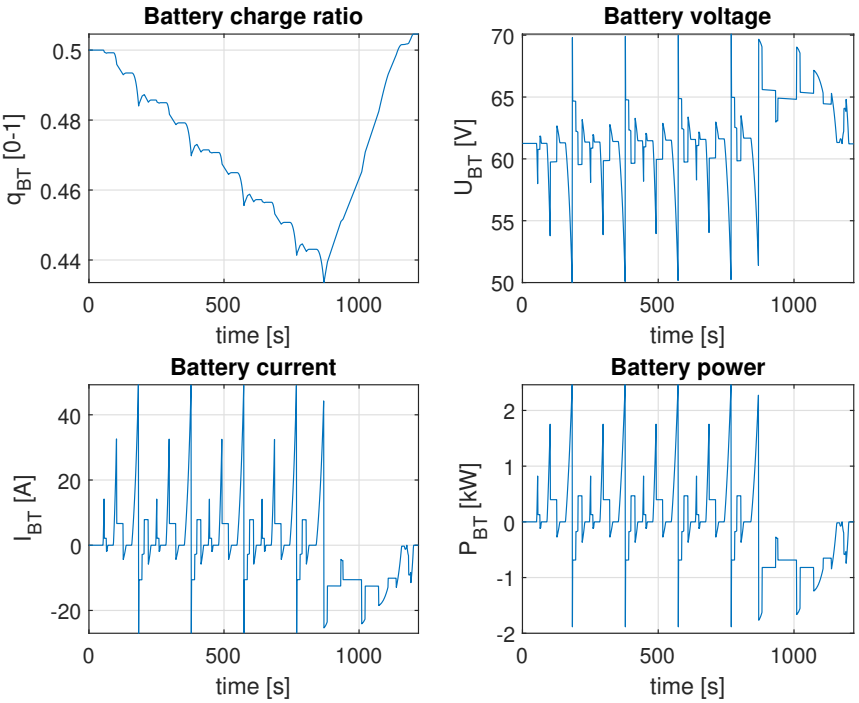

Figure 4.22 Battery States Variation in PHEV Design With EM Connected to Sun Gear, Running on NEDC

The Figures 4.24, 4.25 and 4.26 shows the difference in fuel rate and fuel consumption between the conventional vehicle (Figure 4.24) and PHEV designs (Figure 4.25 for CE connected to ring and Figure4.26 for CE connected to sun) running on NEDC driving cycle. Aggregative fuel consumption indicates the CE is mostly switched off for the first two thirds of the test and mostly switched on for the last one thirds, delivering power both to the wheels and to the EM to recharge the battery to help reach the initial SoC.

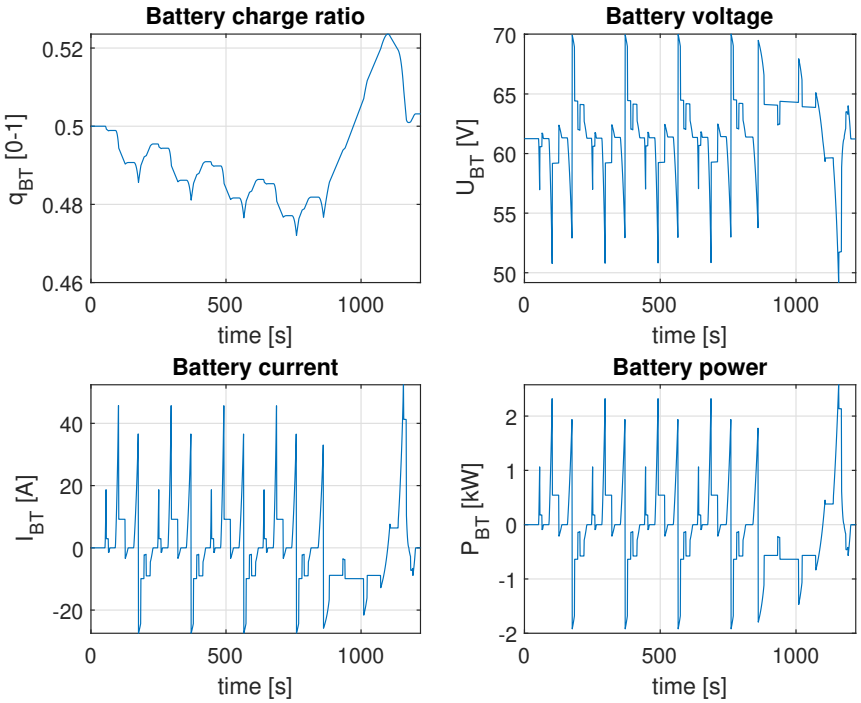

Figure 4.23 Battery States Variation in PHEV Design With EM Connected to Ring Gear, Running on NEDC

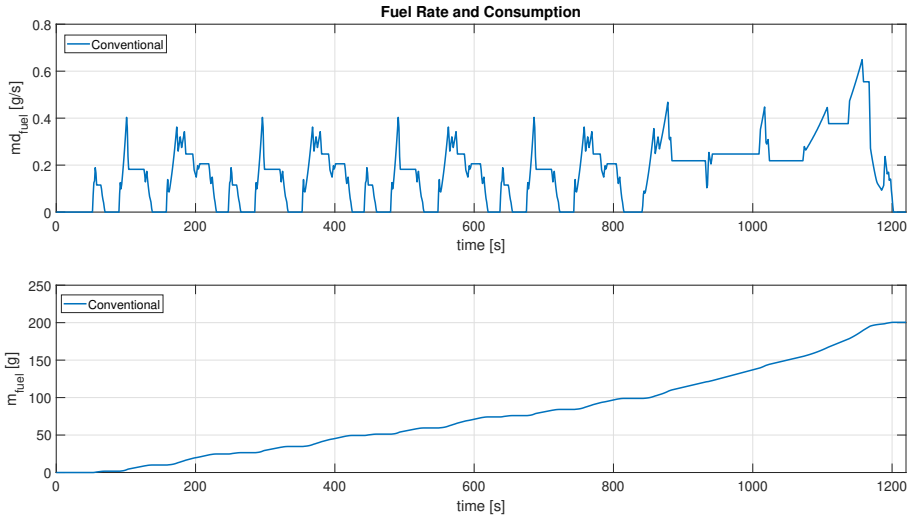

Figure 4.24 Fuel Consumption of Conventional Powertrain Running on NEDC

In Table 4.4, the summary of the fuel consumption of CE in all configurations, including conventional, PHEV with CE connected to ring and sun gears are shown. The results indicate that in the NEDC driving cycle, the conventional vehicle requires 200.45

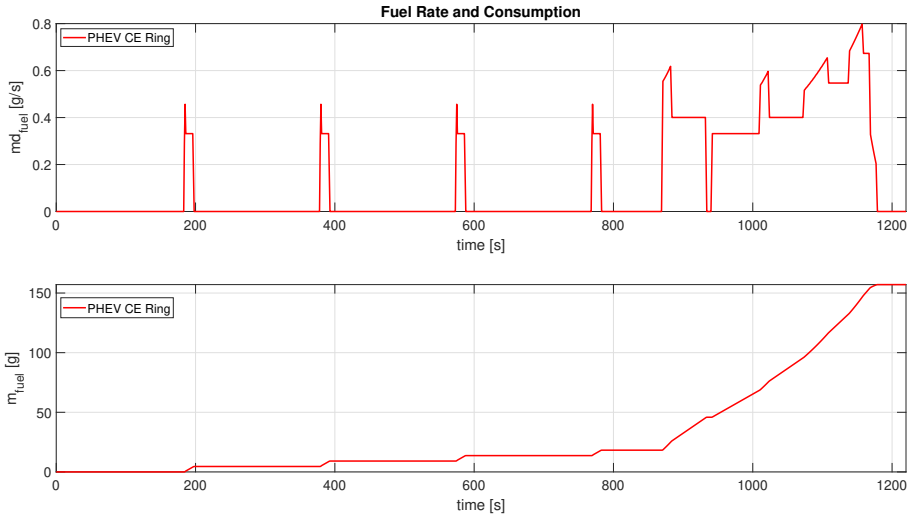

Figure 4.25 Fuel Consumption of PHEV With CE Connected to Ring Gear Running on NEDC

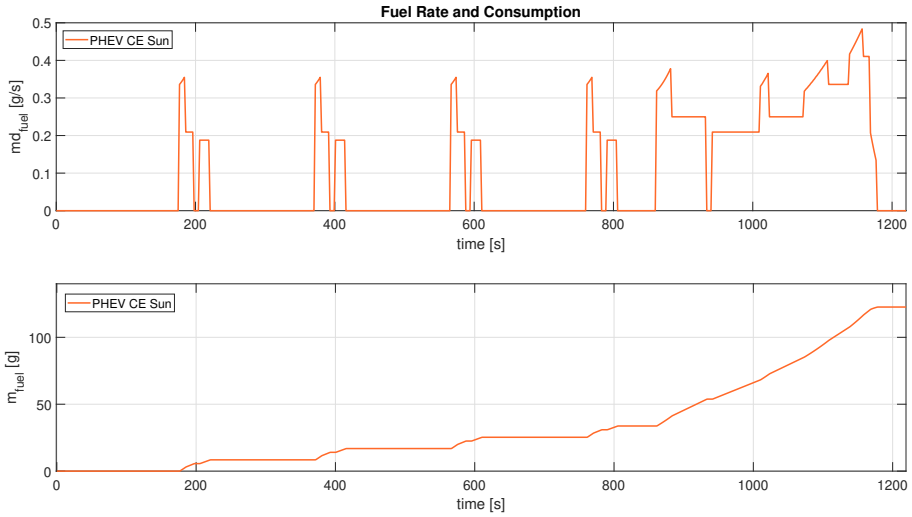

Figure 4.26 Fuel Consumption of PHEV With CE connected to Sun Gear Running on NEDC

grams of fuel while for the PHEV architectures require less fuel for both applications. For CE connected to ring gear, the fuel consumption reduces to 157.07 grams. For CE connected to sun gear, the fuel consumption reduces to 122.63 grams. These results indicate some important details. First, for either application, a fuel consumption reduction figures are achieved for both architectures, despite less than ideal efficiency values for both powerlines of the gearbox. The second detail is the importance of the efficiency values of the gearbox. If the CE is connected to the ring side of the gear-

box, where the efficiency was calculated as $\mu \approx 0.6$, a fuel consumption reduction of $\approx$22% is achieved. However, if the CE is connected to the sun side of the gearbox, with an extra reduction gear applied to the EM for its operation, where the efficiency was calculated as $\mu \approx 0.8$, a fuel consumption reduction of $\approx$39% is achieved. This shows that connecting the CE to the more efficient region, which is determined to be the Sun-Carrier powerline ($P_2 - P_3$). These numbers can be further enhanced with the use of different control strategies.

Table 4.4 Fuel Consumption and Economy Values for Both Powertrain Designs

Powertrain	**Travel Dist. (km)**	**Fuel Cons. (g)**	**Fuel econ. (L/100km)**	**Fuel Cons. Reduction**
Conventional	10.92	200.45	2.46	-
PHEV, CE Ring	10.92	157.07	1.99	22%
PHEV, CE Sun	10.92	122.63	1.51	39%

CHAPTER 5

CONCLUSION

5.1. Conclusion

A mathematical model was constructed using an example gearbox design with Goodman Criterion. After it was validated, it was modified to fit our purposes. The aim was to determine the wear and bending safety factors for the gears and the safety factors on the critical points on the shafts. In conclusion, the parts were designed to meet our safety criteria using a custom mathematical model, which sped up the calculation process as it was made possible to make small alterations on the design and validate the safety of the parts very easy. First, a mathematical model was created using an example gearbox design and its validity was double checked. Second, it was modified to be compatible with a planetary gearbox system which would be used in hybridization of an existing ICE powertrain. With this model, a new planetary gearbox was constructed and properties of each mechanical part was determined. With the results, it was made possible to create an accurate 3D CAD model for the gearbox which could satisfy our requirements. Then, technical drawings were created and the production phase began. The parts are manufactured and the assembly procedure is completed. The dynamometer inertia, along with the EM efficiency map was determined. The gearbox has been connected to the dynamometer and its efficiency map for the power flows were determined. For $P_1 - P_3$, the efficiency was determined to be $\approx 60\%$, and for $P_2 - P_3$, the efficiency was determined to be $\approx 80\%$

A Parallel Hybrid Electric Vehicle (PHEV) model was developed in this study, and it was validated by a similar hybrid electric example of open-source QSS-Toolbox in MATLAB/Simulink. The model parameters were adapted for 1/5 scale passenger vehicle requirements. The gearbox properties, along with its efficiency, was determined first using the described methods and were inserted here. The purpose was to determine how much fuel consumption could be reduced by hybridizing an existing CE power unit. The fuel consumption for this application was determined by using a Simulink model, which made it possible to accurately determine the fuel consumption values for hybrid vehicles. In first part of application, a 1/5 scaled vehicle Simulink model

was constructed. Second, it was adapted for hybrid application by adding a planetary gearbox for the mechanical coupling. Third, the European NEDC driving cycle was integrated to the Simulink model for real-life driving cycles. The results showed that the two different PHEV setups had different fuel consumption reduction values despite the CEs running on similar RPM, power and load values. If the CE is connected to the ring side of the gearbox, a fuel consumption reduction of ≈22% is achieved and if the CE is connected to the sun side of the gearbox, a fuel consumption reduction of ≈39% is achieved in a realistic urban driving cycle, showing the potential of hybridization in real-life applications.

5.2. Recommendations for Future Works

With the efficiency of the gearbox known, along with the hybrid powertrain fuel consumption benefits, the ICE could be connected to the gearbox after its repair process is finished to create a hybrid powertrain to prove the simulation findings. A control algorithm could be developed for the hybrid powertrain to optimize the points for ICE and EM power inputs to minimize the fuel consumption value.

For the future prototypes that will be assembled into vehicle body, the design of the gearbox should be modified considering the available space in powerline and the efficiency values of the different power flow directions of the gearbox. A possible way to improve efficiency is to have the gearbox manufactured professionally to minimize or eliminate any possibilites that could be caused by manufacturing or assembly defects. Another possibility is to improve the oiling system of the gearbox by using one or more oil pumps and oil jets to ensure complete lubrication is applied to every mechanical part of the gearbox.

REFERENCES

[1] B. E. Layton, "A comparison of energy densities of prevalent energy sources in units of joules per cubic meter," *International Journal of Green Energy*, vol. 5, no. 6, pp. 438–455, 2008.

[2] A. Albatayneh, M. N. Assaf, D. Alterman, and M. Jaradat, "Comparison of the Overall Energy Efficiency for Internal Combustion Engine Vehicles and Electric Vehicles," *Environmental and Climate Technologies*, vol. 24, no. 1, pp. 669–680, Jan. 2020.

[3] D. S. Puma-Benavides et al., "Comparative Analysis of Energy Consumption between Electric Vehicles and Combustion Engine Vehicles in High-Altitude Urban Traffic," *World Electric Vehicle Journal*, vol. 15, no. 8, p. 355, Aug. 2024.

[4] G. Belingardi and A. Scattina, "Battery Pack and Underbody: Integration in the Structure Design for Battery Electric Vehicles—Challenges and Solutions," *Vehicles*, vol. 5, no. 2, pp. 498–514, Jun. 2023.

[5] A. A. Naqvi, A. Zahoor, A. A. Shaikh, F. A. Butt, F. Raza, and I. U. Ahad, "Aprotic lithium air batteries with oxygen-selective membranes," *Mater Renew Sustain Energy*, vol. 11, no. 1, pp. 33–46, Jan. 2022.

[6] C. E. Thomas, "Fuel cell and battery electric vehicles compared," *International Journal of Hydrogen Energy*, vol. 34, no. 15, pp. 6005–6020, 2009.

[7] L. Lu, X. Han, J. Li, J. Hua, and M. Ouyang, "A review on the key issues for lithium-ion battery management in electric vehicles," *Journal of Power Sources*, vol. 226, pp. 272–288, Mar. 2013.

[8] J. W. Brennan and T. E. Barder, "Battery Electric Vehicles vs . Internal Combustion Engine Vehicles : A United States-Based Comprehensive Assessment," Arthur D. Little, Tech. Rep., Nov. 2016, pp. 1–48.

[9] T. R. Hawkins, B. Singh, G. Majeau-Bettez, and A. H. Strømman, "Comparative Environmental Life Cycle Assessment of Conventional and Electric Vehicles," *Journal of Industrial Ecology*, vol. 17, no. 1, pp. 53–64, 2013.

[10] C. R. Hung, S. Völler, M. Agez, G. Majeau-Bettez, and A. H. Strømman, "Regionalized climate footprints of battery electric vehicles in Europe," *Journal of Cleaner Production*, vol. 322, p. 129 052, Nov. 2021.

[11] E. Pipitone, S. Caltabellotta, and L. Occhipinti, "A life cycle environmental impact comparison between traditional, hybrid, and electric vehicles in the european context," *Sustainability*, vol. 13, no. 19, p. 10 992, Oct. 2021.

[12] Y. Ligen, H. Vrubel, and H. H. Girault, "Mobility from renewable electricity: Infrastructure comparison for battery and hydrogen fuel cell vehicles," *World Electric Vehicle Journal*, vol. 9, no. 1, p. 3, May 2018.

[13] H. Togun et al., "Development and comparative analysis between battery electric vehicles (BEV) and fuel cell electric vehicles (FCEV)," *Applied Energy*, vol. 388, p. 125 726, Jun. 2025.

[14] Toyota Motor Corporation, "Contrasts in Value and Manufacturing – The Second-Generation Mirai and New GR Yaris," *Toyota Technical Review*, vol. 66, no. 236, pp. 4–188, Mar. 2021.

[15] D. L. Greene, J. M. Ogden, and Z. Lin, "Challenges in the designing, planning and deployment of hydrogen refueling infrastructure for fuel cell electric vehicles," *eTransportation*, vol. 6, p. 100 086, Oct. 2020.

[16] T. Burton, S. Powers, C. Burns, G. Conway, F. Leach, and K. Senecal, "A Data-Driven Greenhouse Gas Emission Rate Analysis for Vehicle Comparisons," *SAE International Journal of Electrified Vehicles*, vol. 12, no. 1, pp. 1–37, Apr. 2022.

[17] Y. Liu, Y. G. Liao, and M. C. Lai, "Fuel economy improvement and emission reduction of 48 V mild hybrid electric vehicles with P0, P1, and P2 architectures with lithium battery cell experimental data," *Advances in Mechanical Engineering*, vol. 13, no. 10, pp. 1–10, Oct. 2021.

[18] M. Ehsani, Y. Gao, S. Longo, and K. M. Ebrahimi, *Modern Electric, Hybrid Electric, and Fuel Cell Vehicles*. Boca Raton, FL, USA: CRC Press, Taylor & Francis Group, 2018, vol. 1, pp. 1–546.

[19] M. De Carlo and G. Mantriota, "Electric vehicles with two motors combined via planetary gear train," *Mechanism and Machine Theory*, vol. 148, p. 103 789, Jun. 2020.

[20] M. Bozca, "Optimisation of Effective Design Parameters for an Automotive Transmission Gearbox to Reduce Tooth Bending Stress," *Modern Mechanical Engineering*, vol. 07, no. 02, pp. 35–56, May 2017.

[21] C.-Y. C. Lin and L. Prince, "Gasoline price volatility and the elasticity of demand for gasoline," Department of Agricultural and Resource Economics, University of California, Davis, Tech. Rep., 2012, pp. 1–19.

[22] K. Kpodar and C. Abdallah, "Dynamic fuel price pass-through: Evidence from a new global retail fuel price database," *Energy Economics*, vol. 66, pp. 303–312, Aug. 2017.

[23] P. Jaramillo, S. K. Ribeiro, and P. Newman, "Transport," in *Climate Change 2022 - Mitigation of Climate Change*, P. R. Shukla et al., Eds., 1st ed., vol. 1, Cambridge University Press, Aug. 2023, ch. 10, pp. 1049–1160.

[24] J. Fan, X. Meng, J. Tian, C. Xing, C. Wang, and J. Wood, "A review of transportation carbon emissions research using bibliometric analyses," *Journal of Traffic and Transportation Engineering (English Edition)*, vol. 10, no. 5, pp. 878–899, Oct. 2023.

[25] Z. Hussain, B. Marcel, A. Majeed, and R. S. M. Tsimisaraka, "Effects of transport–carbon intensity, transportation, and economic complexity on environmental and health expenditures," *Environment, Development and Sustainability*, vol. 26, no. 7, pp. 16 523–16 553, Jul. 2024.

[26] S. Rashid and E. Pagone, “Cradle-to-Grave Lifecycle Environmental Assessment of Hybrid Electric Vehicles,” *Sustainability (Switzerland)*, vol. 15, no. 14, pp. 1–23, Jul. 2023.

[27] G. Wu, A. Inderbitzin, and C. Bening, “Total cost of ownership of electric vehicles compared to conventional vehicles: A probabilistic analysis and projection across market segments,” *Energy Policy*, vol. 80, pp. 196–214, May 2015.

[28] A. Nordelöf, M. Messagie, A. M. Tillman, M. Ljunggren Söderman, and J. Van Mierlo, “Environmental impacts of hybrid, plug-in hybrid, and battery electric vehicles—what can we learn from life cycle assessment?” *International Journal of Life Cycle Assessment*, vol. 19, no. 11, pp. 1866–1890, Aug. 2014.

[29] Y. Zhang, Z. Cao, C. Zhang, and Y. Chen, “Life Cycle Assessment of Plug-In Hybrid Electric Vehicles Considering Different Vehicle Working Conditions and Battery Degradation Scenarios,” *Energies*, vol. 17, no. 17, pp. 1–29, Aug. 2024.

[30] G. Bieker, “A Global Comparison Of The Life-Cycle Greenhouse Gas Emissions Of Combustion Engine And Electric Passenger Cars,” ICCT White Paper, Tech. Rep., Jul. 2021, pp. 1–81.

[31] K. Petrauskienė, A. Galinis, D. Kliaugaitė, and J. Dvarionienė, “Comparative environmental life cycle and cost assessment of electric, hybrid, and conventional vehicles in Lithuania,” *Sustainability (Switzerland)*, vol. 13, no. 2, pp. 1–17, Jan. 2021.

[32] L. B. Lave and H. L. Maclean, “An environmental-economic evaluation of hybrid electric vehicles: Toyota’s Prius vs. its conventional internal combustion engine Corolla,” *Transportation Research Part D*, vol. 6, no. 7, pp. 155–162, Jan. 2002.

[33] A. Benevieri et al., “Series architecture on hybrid electric vehicles: A review,” *Energies*, vol. 14, no. 22, pp. 1–31, Nov. 2021.

[34] L. B. Rana, A. Shrestha, S. Phuyal, B. Mali, O. Lakhey, and R. K. Maskey, "Design and performance evaluation of series hybrid electric vehicle using backward model," *The Journal of Engineering*, vol. 2020, no. 11, pp. 1095–1102, Nov. 2020.

[35] Y. Pan et al., "A Review of Hybrid Vehicles Classification and Their Energy Management Strategies: An Exploration of the Advantages of Genetic Algorithms," *Algorithms*, vol. 18, no. 6, pp. 1–40, Jun. 2025.

[36] P. Dong et al., "Performance comparison of series–parallel hybrid transmissions with multiple gears and modes based on efficiency model," *Energy Conversion and Management*, vol. 274, p. 116 442, Dec. 2022.

[37] C.-T. Li, X. Zhang, and H. Peng, "Design of Power-Split Hybrid Vehicles With a Single Planetary Gear," in *Proceedings of the ASME 2012 5th Annual Dynamic Systems and Control Conference jointly with the JSME 2012 11th Motion and Vibration Conference (DSCC2012-MOVIC2012)*, Oct. 2012, pp. 1–9.

[38] J. Wei et al., "A coupling dynamics analysis method for a multistage planetary gear system," *Mechanism and Machine Theory*, vol. 110, pp. 27–49, Apr. 2017.

[39] D. Bonev and A. Dobreva, "Analysis of planetary gear trains applied in vehicles," *International Scientific Journal Trans \& Motauto World*, no. 1, pp. 5–8, Jan. 2023.

[40] C. A. González-Cruz and M. Ceccarelli, "Experimental characterization of the coupling stage of a two-stage planetary gearbox in variable operational conditions," *Machines*, vol. 7, no. 2, p. 45, Jun. 2019.

[41] M. Molaie, S. Deylaghian, G. Iarriccio, F. S. Samani, A. Zippo, and F. Pellicano, "Planet Load-Sharing and Phasing," *Machines*, vol. 10, no. 8, pp. 1–29, Jul. 2022.

[42] H. Wang, T. Zhang, G. Liu, and L. Wu, "System-structure coupling dynamic analysis of planetary gears," *Mathematical Problems in Engineering*, vol. 2015, pp. 1–10, May 2015.

[43] S. Janigová and B. Schürger, "Design Optimization of the Modified Planetary Carrier," *Journal of Engineering Sciences*, vol. 8, no. 1, pp. 17–22, May 2021.

[44] J. Keller, Y. Guo, Z. Zhang, and D. Lucas, "Comparison of planetary bearing load-sharing characteristics in wind turbine gearboxes," *Wind Energy Science*, vol. 3, no. 2, pp. 947–960, Dec. 2018.

[45] F. Verbelen, P. Defreyne, P. Sergeant, and K. Stockman, "Efficiency Measurement Strategy for a Planetary Gearbox with 2 Degrees of Freedom," in *Proceedings of the International Conference on Electrical Machines (ICEM)*, Jan. 2018, pp. 1–8.

[46] L. Wang, Y. Cui, F. Zhang, and G. Li, "Architectures of planetary hybrid powertrain system: Review, classification and comparison," *Energies*, vol. 13, no. 2, pp. 1–24, Jan. 2020.

[47] R. G. Budynas, J. K. Nisbett, and J. E. Shigley, *Shigley's mechanical engineering design*. New York, NY, United States of America: McGraw-Hill, 2011, pp. 1–1082.

[48] F. Lopot et al., "Gearbox mechanical efficiency determination by strain gauges direct application," *Applied Sciences*, vol. 11, no. 23, p. 11 150, Nov. 2021.

[49] T. Petr, J. Brousek, J. Jezek, T. Zvolsky, and R. Vozenilek, "Measuring the Efficiency of Reduction Gearboxes for Electric Utility Vehicles during Specific Driving Cycles," *Strojniski Vestnik/Journal of Mechanical Engineering*, vol. 68, no. 5, pp. 303–313, 2022.

[50] J. Li, C.-C. Li, and J. Huang, "Transmission Efficiency Analysis and Experiment Research of Gear Box," in *Proceedings of the 3rd Annual International Conference on Mechanics and Mechanical Engineering (MME 2016)*, Atlantis Press, Dec. 2016, pp. 298–303.

[51] S. Dereyne, P. Defreyne, E. Algoet, and S. Derammelaere, "Efficiency Measurement Campaign on Gearboxes," in *Proceedings of the 9th International Confer-*

ence on Energy Efficiency in Motor Driven Systems (EEMODS 2015), Jan. 2015, pp. 1–11.

[52] G. Shi, H. Ban, Y. Bai, Y. Wang, C. Luo, and Y. Shi, "A novel cast aluminum joint for reticulated shell structures: Experimental study and modeling," *Advances in Structural Engineering*, vol. 16, no. 6, pp. 1047–1060, Jun. 2013.

[53] P. Bałon, E. Rejman, R. Smusz, J. Szostak, and B. Kiełbasa, "Implementation of high speed machining in thin-walled aircraft integral elements," *Open Engineering*, vol. 8, no. 1, pp. 162–169, Jun. 2018.

[54] International Organization for Standardization, "ISO 6336-2 Calculation of load capacity of spur and helical gears-Part 2: Calculation of surface durability (pitting)," ISO, Tech. Rep., Sep. 2006, pp. 1–7.

[55] Yamaha Motor da Amazônia Ltda, "YAMAHA YBR250 Technical DataSheet," Yamaha Motor Company, Tech. Rep., Jan. 2007, pp. 1–68.

[56] L. Guzzella and A. Amstutz, "The QSS Toolbox Manual," Institut für Mess und Regeltechnik, Tech. Rep., Jun. 2005, pp. 1–63.